Predictions from scoto-seesaw with A_4 modular symmetry

Ranjeet Kumar,[1,*] Priya Mishra,[2,†] Mitesh Kumar
Behera,[3,‡] Rukmani Mohanta,[2,§] and Rahul Srivastava[1,¶]

[1]*Department of Physics, Indian Institute of Science Education and Research - Bhopal,*

Bhopal Bypass Road, Bhauri, Bhopal 462066, India

[2]*School of Physics, University of Hyderabad, Hyderabad - 500046, India*

[3]*Department of Physics, Faculty of Science, Chulalongkorn University, Bangkok-10330, Thailand*

This paper's novelty lies in introducing a hybrid scoto-seesaw model rooted in A_4 discrete modular symmetry leading to several interesting phenomenological implications. The scoto-seesaw framework leads to generation of one mass square difference (Δm_{atm}^2) using the type-I seesaw mechanism at the tree level. Additionally, the scotogenic contribution is vital in obtaining the other mass square difference (Δm_{sol}^2) at the loop level, thus providing a clear interpretation of the two different mass square differences. The non-trivial transformation of Yukawa couplings under the A_4 modular symmetry helps to explore neutrino phenomenology with a specific flavor structure of the mass matrix. In addition to predictions for neutrino mass ordering, mixing angles and CP phases, this setup leads to precise predictions for $\sum m_i$ as well as $|m_{ee}|$. In particular, the model predicts $\sum m_i \in (0.073, 0.097)$ eV and $|m_{ee}| \in (3.15, 6.66) \times 10^{-3}$ eV range; within reach of upcoming experiments. Furthermore, our model is also promising for addressing lepton flavor violations, i.e., $\ell_\alpha \to \ell_\beta \gamma$, $\ell_\alpha \to 3\ell_\beta$ and $\mu - e$ conversion rates while staying within the realm of current experimental limits.

1. INTRODUCTION

The Standard Model (SM) falls short to provide complete understanding of the properties of neutrinos. Instead of being strictly massless as predicted in the SM, neutrinos have been observed to

* ranjeet20@iiserb.ac.in

† mishpriya99@gmail.com

‡ miteshbehera1304@gmail.com

§ rmsp@uohyd.ac.in

¶ rahul@iiserb.ac.in

possess extremely small but non-zero masses through neutrino oscillation data [1]. This phenomenon has solidified the evidence for neutrino mixing, indicating that at least two neutrinos have non-zero masses [2–5]. Theoretically and experimentally, neutrinos lack right-handed counterparts in the SM, making it unlikely for them to acquire masses through the Higgs mechanism like other charged fermions. However, the presence of a dimension-five Weinberg operator [6–8] can offer a viable means for neutrino mass generation. Nevertheless, the origin and flavor structure of this operator remains debatable. Hence, it is crucial to explore scenarios beyond the standard model (BSM) to account for neutrinos' non-zero masses. Numerous models have been proposed in the literature to explain the experimental data from various neutrino oscillation experiments. One popular mechanism is the seesaw mechanism [9–11], and other models include radiative mass generation [12, 13], extra dimensions [14–18], etc., among others. A common feature in many BSM scenarios that can generate non-zero neutrino masses is the existence of sterile neutrinos, which are gauge singlets under the SM and are often referred to as right-handed neutrinos. They are connected to the standard active neutrinos through Yukawa interactions. These sterile neutrinos' masses and interaction strengths can vary over several orders of magnitude, leading to a wide range of observable phenomena.

For instance, within the canonical seesaw framework, the right-handed neutrino mass is expected to be around 10^{15} GeV to explain the eV-scale light neutrinos. However, this mass scale is far beyond the reach of current and future experiments. Nonetheless, there are other variants of the seesaw mechanism, such as inverse seesaw [19–24], linear seesaw [25–33], extended seesaw [34, 35], have been proposed by using certain discrete [36–49] and/or continuous symmetries [50–56], where the heavy neutrino mass can be in the TeV range, making them experimentally testable. To date, the only measured neutrino mass parameters are the two mass square differences linked to the oscillations of "atmospheric" and "solar" neutrinos [57, 58]. The presence of these two distinct mass scales might suggest that the origins of these two scales stem from separate mechanisms [59].

To validate our assertions, we employ a recently proposed idea of modular symmetry [60–63]. Some of the current effective models based on discrete flavor symmetry along with modular symmetry, which have been recently put forward [64, 65], do not incorporate flavon fields except for the modulus τ. Consequently, the flavor symmetry is broken when the complex modulus τ obtains a vacuum expectation value (VEV). This approach avoids the use of perplexing vacuum alignment and requires a mechanism to determine the modulus τ. Consequently, this framework alters Yukawa couplings, wherein these couplings being dependent on modular forms, which are

essentially holomorphic functions of τ. In other words, these couplings manifest within a non-trivial representation of a non-Abelian discrete flavor symmetry, compensating for the need for flavon fields, which are not essential or are minimized for achieving the desired flavor structure. In the aforementioned context, an extensive review of various literature sources reveals the existence of numerous groups based on the modular group, including S_3 [66–68], A_4 [37, 69–85], S_4 [86–92], and A_5 [93, 94], along with more expansive groups [95], various other modular symmetries, and the double covering of A_4 [96–98] and A_5 [23, 26, 99] symmetry. These groups enable predictions to be made regarding the masses, mixing patterns, and CP phases specific to quarks and/or leptons [100–103].

In this paper, we introduce a scotogenic extension of the basic canonical seesaw mechanism, which offers a straightforward explanation for the two distinct oscillation scales and their corresponding messengers that have been observed. Initially, we focus solely on generating the atmospheric scale through the exchange of singlet right-handed (RH) neutrinos, as found in the minimal type-I seesaw mechanism. At this point, two neutrinos remain without mass, resulting in the absence of solar neutrino oscillations. However, we subsequently demonstrate that this degeneracy in mass can be resolved through predictable scotogenic-type radiative corrections leading to a hybrid seesaw called "scoto-seesaw" which is the first of its kind because of the implementation of modular symmetry.

The structure of this paper is as follows. In Sec. 2, we outline the theoretical framework of the scoto-seesaw mechanism with discrete A_4 modular flavor symmetry and its appealing features resulting in simple mass structure for the charged leptons and neutral leptons including light active neutrinos and other two types of sterile neutrinos. Then we discuss the light neutrino masses and mixing in this framework. In Sec. 3, a numerical correlational study between observables of the neutrino sector and model input parameters is established. We also present a brief discussion on lepton flavor violation in Sec. 4, and in Sec. 5, we conclude our results.

2. MODEL FRAMEWORK

This section is curated to discuss the formalism involved in describing the model framework, which is based on modular A_4 symmetry in the supersymmetric context. To ensure the minimal charge assignment of superfields, we have considered zero modular weight for two Higgs doublets H_u and H_d as well as for charged leptons L_ℓ, ℓ_R^c ($\ell = e, \mu, \tau$). Higgs doublets are trivial singlets under A_4 symmetry. The charged leptons are singlet representations of A_4, while L_ℓ and ℓ_R^c are assigned as $(1, 1', 1'')$ and $(1, 1'', 1')$ respectively. This setup leads the charged lepton mass matrix

to be diagonal, which can be obtained after applying the A_4 product rule (see App. B). Therefore, leptonic mixing matrix can arise solely from the diagonalization of the neutrino mass matrix. To produce the two different mass scales of neutrino oscillation, we have considered the scoto-seesaw setup [104–108], where neutrino mass will be generated at tree level from type-I seesaw and from scoto-loop [109]. For the type-I seesaw mechanism, we have incorporated two new superfields N_{R_1} and N_{R_2} with modular weight, $k = 4$, and they transform as 1 and 1′ under A_4 respectively. In the case of the scoto-loop scenario, we have introduced additional superfields f and η with weight $k = 5$ and $k = 3$, respectively, and they both transform as trivial singlet (1) of A_4. We have added another scalar superfield η' to cancel the gauge anomaly [1]. The charge assignment of the superfields and their weights, as well as relevant modular Yukawas, are summarized in Tab. I.

Fields	Fermions					Scalars			Yukawa couplings					
	L_ℓ	ℓ_R^c	N_{R_1}	N_{R_2}	f	$H_{u,d}$	η	η'	$Y_1^{(4)}$	$Y_{1'}^{(4)}$	$Y_1^{(8)}$	$Y_{1'}^{(8)}$	$Y_{1''}^{(8)}$	$Y_1^{(10)}$
$SU(2)_L$	2	1	1	1	1	2	2	2	–	–	–	–	–	–
$U(1)_Y$	$-1/2$	1	0	0	0	$\pm 1/2$	$1/2$	$-1/2$	–	–	–	–	–	–
A_4	$1, 1', 1''$	$1, 1'', 1'$	1	1′	1	1	1	1	1	1′	1	1′	1″	1
k_I	0	0	4	4	5	0	3	3	4	4	8	8	8	10

TABLE I: Particle content and modular Yukawa couplings of the model and their charges under $SU(2)_L \times U(1)_Y \times A_4$, where k_I is the number of modular weight.

The weight and representation of superfields are chosen so that only the superfields f and η can appear at loop level. This property holds because Yukawas can have only even weight under A_4 modular symmetry. To ensure that there is no mixing between the tree and loop level BSM superfields, we have assigned even and odd weights to the tree and loop level BSM superfields, respectively. The above-discussed condition is basically that H_u and η have the same hypercharge that will allow H_u to appear at loop level and η to appear at that tree level, but the assignment of even and odd weight for H_u and η respectively restrict this choice. This analogy also applies to tree level and loop level fermions N_{R_1}, N_{R_2} and f, respectively. The leptonic mass matrices are restricted due to specific charge assignment and weight, as discussed below.

---

[1] Note that the superfield η' will not play any active role in neutrino mass generation.

Charged lepton and neutrino mass matrices

The charge assignment of leptons (L_ℓ, ℓ_R^c) as given in Tab. I, allows us to have the following superpotential mentioned below:

$$\mathcal{W}_{M_\ell} = y_\ell^{ee} L_e H_d e_R^c + y_\ell^{\mu\mu} L_\mu H_d \mu_R^c + y_\ell^{\tau\tau} L_\tau H_d \tau_R^c . \tag{1}$$

The above superpotential leads to a diagonal matrix after the application of the A_4 product rule (see App. B).

$$M_\ell = \begin{pmatrix} y_\ell^{ee} v_d & 0 & 0 \\ 0 & y_\ell^{\mu\mu} v_d & 0 \\ 0 & 0 & y_\ell^{\tau\tau} v_d \end{pmatrix} \equiv \begin{pmatrix} m_e & 0 & 0 \\ 0 & m_\mu & 0 \\ 0 & 0 & m_\tau \end{pmatrix} . \tag{2}$$

Here, v_d is VEV of H_d and m_e, m_μ, and m_τ are the observed charged lepton masses.

To generate the neutrino masses, we have adopted a scoto-seesaw scenario [59]. Hence, we will have contributions from both tree and loop levels[2] in the neutrino sector as shown in Fig. 1, where we have taken superpartners to be very heavy. Considering the charge assignments and weights of
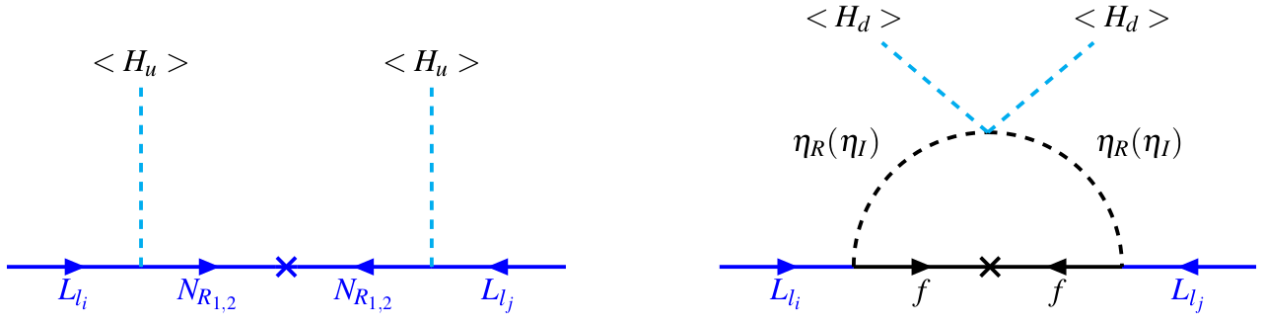

FIG. 1: Neutrino mass generation from "scoto-seesaw" mechanism. The left diagram corresponds to the tree level seesaw while the right diagram represents the effective one loop scotogenic contribution to neutrino masses.

superfields given in Tab. I, the most general superpotential allowed by A_4 modular symmetry can

---

[2] To generate neutrino masses through the scotogenic mechanism at loop level one needs mass splitting between real and imaginary components of η (η_R and η_I). In SUSY framework the term $(\eta^\dagger H_u)^2$ which provides mass splitting is not allowed. But one can generate this mass splitting through effective interaction. (see App. A).

be expressed as:

$$\mathcal{W}_\nu^T = \alpha_1 Y_1^{(4)} L_e H_u N_{R_1} + \alpha_2 Y_{1'}^{(4)} L_\tau H_u N_{R_1} + \alpha_3 Y_{1'}^{(4)} L_\mu H_u N_{R_2} + \alpha_4 Y_1^{(4)} L_\tau H_u N_{R_2}$$
$$+ \kappa_1 Y_1^{(8)} N_{R_1} N_{R_1} + \kappa_2 Y_{1''}^{(8)} N_{R_2} N_{R_2} + \kappa_{12} Y_{1'}^{(8)} N_{R_1} N_{R_2}. \tag{3}$$

For the minimal choice of the parameters in our model, we have considered all α's to be the same i.e. α_T and $\kappa_1, \kappa_2 \gg \kappa_{12}$. Hence, the above superpotential modifies as:

$$\mathcal{W}_\nu^T = \alpha_T \left(Y_1^{(4)} L_e H_u N_{R_1} + Y_{1'}^{(4)} L_\tau H_u N_{R_1} + Y_{1'}^{(4)} L_\mu H_u N_{R_2} + Y_1^{(4)} L_\tau H_u N_{R_2} \right)$$
$$+ \kappa_1 Y_1^{(8)} N_{R_1} N_{R_1} + \kappa_2 Y_{1''}^{(8)} N_{R_2} N_{R_2}. \tag{4}$$

At the tree level, matrices M_D and M_R are as follows:

$$M_D = \begin{pmatrix} Y_1^{(4)} & 0 \\ 0 & Y_{1'}^{(4)} \\ Y_{1'}^{(4)} & Y_1^{(4)} \end{pmatrix} \alpha_T v_u, \qquad M_R = \begin{pmatrix} \kappa_1 Y_1^{(8)} & 0 \\ 0 & \kappa_2 Y_{1''}^{(8)} \end{pmatrix}, \tag{5}$$

where, v_u is the VEV of H_u. Thus, considering the type-I seesaw formula, one can obtain the light neutrino mass matrix at the leading order as

$$(M_\nu)_{\text{tree}} = -M_D M_R^{-1} M_D^T . \tag{6}$$

Using the expressions of M_D and M_R from (5), we will have

$$(M_\nu)_{\text{tree}} = -(\alpha_T v_u)^2 \begin{pmatrix} A & 0 & p\sqrt{AB} \\ 0 & B & r\sqrt{AB} \\ * & * & p^2 B + r^2 A \end{pmatrix}, \tag{7}$$

where, $\sqrt{A} = Y_1^{(4)} \sqrt{\frac{1}{M_1}}$, $\sqrt{B} = Y_{1'}^{(4)} \sqrt{\frac{1}{M_2}}$, $p = \sqrt{\frac{M_2}{M_1}}$, $r = \sqrt{\frac{M_1}{M_2}}$ and $M_1 \approx \kappa_1 Y_1^{(8)}$, $M_2 \approx \kappa_2 Y_{1''}^{(8)}$. The neutrino mass term can also be generated at one loop level through the scotogenic process due to the presence of the inert doublet η and the fermion f in the loop. The effective superpotential allowed by A_4 modular symmetry is given by,

$$\mathcal{W}_\nu^L = \beta_1 Y_1^{(8)} L_e \eta f + \beta_2 Y_{1''}^{(8)} L_\mu \eta f + \beta_3 Y_{1'}^{(8)} L_\tau \eta f + \kappa_S Y_1^{(10)} f f , \tag{8}$$

For the minimal choice, we have taken all β's to be the same i.e. β_L, then the above superpotential can be written as:

$$\mathcal{W}_\nu^L = \beta_L \left(Y_1^{(8)} L_e \eta f + Y_{1''}^{(8)} L_\mu \eta f + Y_{1'}^{(8)} L_\tau \eta f \right) + \kappa_S Y_1^{(10)} f f \, , \tag{9}$$

where, β_L and κ_S are the free parameters. The neutrino masses generated effectively at the one loop level can be expressed as follows:

$$\left(M_\nu^{ij} \right)_{\text{loop}} = \mathcal{F} \left(m_{\eta_R}, m_{\eta_I}, M_f \right) M_f \mathbf{h^i h^j} \, , \tag{10}$$

where, $M_f = \kappa_S Y_1^{(10)}$ and the couplings $\mathbf{h^i}$, $\mathbf{h^j}$ are defined as follows:

$$\mathbf{h^1} = \beta_L Y_1^{(8)}, \quad \mathbf{h^2} = \beta_L Y_{1''}^{(8)}, \quad \mathbf{h^3} = \beta_L Y_{1'}^{(8)}, \tag{11}$$

whereas $\mathcal{F} \left(m_{\eta_R}, m_{\eta_I}, M_f \right)$ is the loop function given by:

$$\mathcal{F} \left(m_{\eta_R}, m_{\eta_I}, M_f \right) = \frac{1}{32\pi^2} \left[\frac{m_{\eta_R}^2}{M_f^2 - m_{\eta_R}^2} \ln \left(\frac{M_f^2}{m_{\eta_R}^2} \right) - \frac{m_{\eta_I}^2}{M_f^2 - m_{\eta_I}^2} \ln \left(\frac{M_f^2}{m_{\eta_I}^2} \right) \right] . \tag{12}$$

Hence, the neutrino mass matrix at the loop level evolves as follows:

$$(M_\nu)_{\text{loop}} = \beta_L^2 M_f \begin{pmatrix} \left(Y_1^{(8)} \right)^2 & \left(Y_1^{(8)} Y_{1''}^{(8)} \right) & \left(Y_1^{(8)} Y_{1'}^{(8)} \right) \\ * & \left(Y_{1''}^{(8)} \right)^2 & \left(Y_{1''}^{(8)} Y_{1'}^{(8)} \right) \\ * & * & \left(Y_{1'}^{(8)} \right)^2 \end{pmatrix} \mathcal{F} \left(m_{\eta_R}, m_{\eta_I}, M_f \right) . \tag{13}$$

Using Eqs. (7) and (13), we can write the total contribution of neutrino mass matrix, which is given as

$$M_\nu = (M_\nu)_{\text{tree}} + (M_\nu)_{\text{loop}} \, . \tag{14}$$

Thus, scoto-seesaw mechanism provides not just neutrino masses but also explains the two different observed mass square differences. The presence of A_4 modular symmetry has also interesting phenomenological implications which we will explore next.

3.   RESULTS

In order to perform the numerical analysis, we have utilized the global fit neutrino oscillation data at 3σ interval from [110, 111] as follows.

$$\text{NO}: \Delta m_{\text{atm}}^2 = [2.47, 2.63] \times 10^{-3} \text{ eV}^2, \ \Delta m_{\text{sol}}^2 = [6.94, 8.14] \times 10^{-5} \text{ eV}^2,$$

$$\theta_{13} = [8.13°, 8.92°], \ \theta_{23} = [41.21°, 51.35°], \ \theta_{12} = [31.37°, 37.40°], \ \delta_{\text{CP}}/\pi = [0.71, 1.99]. \quad (15)$$

Here, we numerically diagonalize the neutrino mass matrix Eq. (14) through the relation $U^\dagger \mathcal{M} U = \text{diag}(m_1^2, m_2^2, m_3^2)$, where $\mathcal{M} = M_\nu M_\nu^\dagger$ and U is a unitary matrix, from which the neutrino mixing angles can be extracted using the standard relations:

$$\sin^2 \theta_{13} = |U_{13}|^2, \quad \sin^2 \theta_{12} = \frac{|U_{12}|^2}{1 - |U_{13}|^2}, \quad \sin^2 \theta_{23} = \frac{|U_{23}|^2}{1 - |U_{13}|^2}. \quad (16)$$

The numerical analysis has been done by performing a random scan over the input parameters space given in Tab. II, taking $v_u = v_d$ with $\sqrt{v_u^2 + v_d^2} \approx 174$ GeV. After imposing the observed 3σ limits of solar and atmospheric mass squared differences and further constrained by the mixing angles, the typical range of modulus τ is found to be $0.2 \lesssim |\text{Re}[\tau]| \lesssim 0.5$ and $0.85 \lesssim \text{Im}[\tau] \lesssim 1.3$, satisfying only the normal ordering (NO). In contrast to the above, the present scenario cannot incorporate the inverted ordering (IO) of neutrino mass as briefly discussed in subsection 3.4. Further, we illustrate the results achieved by performing the numerical scan in the following subsections.

We intend to initiate our analysis by embarking focus on the correlations among modular sectors. In support of the above, the left panel of Fig. 2 illustrates a plausible correlation between $\text{Im}[\tau]$ and $\text{Re}[\tau]$. Furthermore, the middle and right panel of Fig. 2 depicts the plausible ranges for modular Yukawa couplings, as well as their associations with $\text{Re}[\tau]$ and $\text{Im}[\tau]$.

3.1.   Neutrino Oscillation Prediction for Normal Ordering

We now proceed to elaborate on the predictions inherent to our model concerning observed neutrino oscillation parameters. Initially, we emphasize a noteworthy aspect of our model, how mixing angles (θ_{23} and θ_{12}) are correlated with complex modulus τ ($\text{Re}[\tau]$ and $\text{Im}[\tau]$) as shown in Fig. 3 (region in green color is 3σ allowed values of θ_{23} and θ_{12}). Proceeding further, in Fig. 3, one can clearly see that in our model, mixing angles have symmetric distribution around the origin for

Input Parameters	Range
Re$[\tau]$	$\pm[0.0, 0.5]$
Im$[\tau]$	$[0.8, 1.5]$
α_T	$[10^{-3}, 10^{-2}]$
β_L	$[10^{-1}, 2]$
M_1 (GeV)	$[1, 10] \times 10^{11}$
M_2 (GeV)	$[1, 10] \times 10^{11}$
M_f (GeV)	$[1, 10^4]$
m_{η_R} (GeV)	$[1, 400]$
m_{η_I} (GeV)	$[1, 400]$

TABLE II: Ranges of the parameters used for the numerical scan.
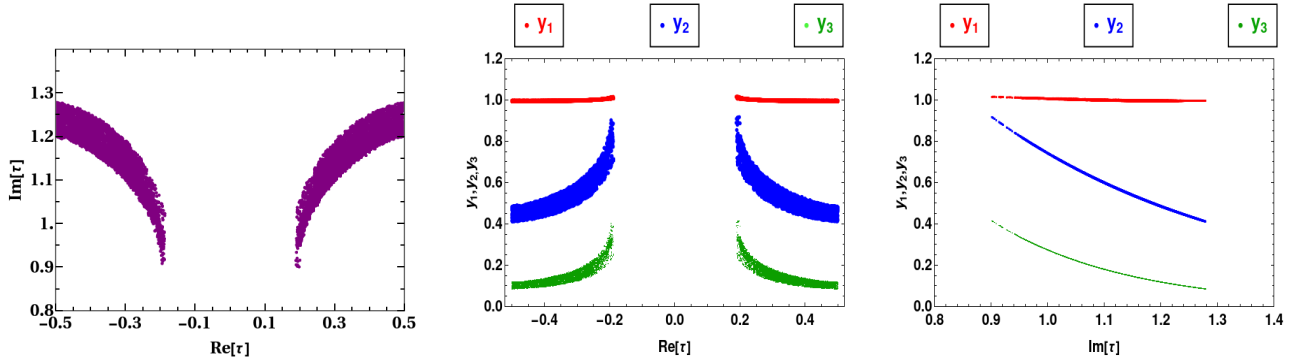
FIG. 2: Left panel corresponds to the correlation between Re$[\tau]$ and Im$[\tau]$, whereas the middle and right panel showcase the correlation of modular Yukawa couplings with Re$[\tau]$ and Im$[\tau]$.

Re$[\tau]$ values. Furthermore, owing to the constraint imposed by θ_{23}, a distinct cutoff region emerges for the Re$[\tau]$ values. Notably, the region $-0.2 \lesssim$ Re$[\tau] \lesssim 0.2$ falls outside the permissible range of θ_{23} as shown in the left panel of Fig. 3. The corollary to this imposition becomes readily evident in the right panel of Fig. 3, wherein the absence of data points within the region $-0.2 \lesssim$ Re$[\tau] \lesssim 0.2$ is manifested due to the prior imposition of the θ_{23} constraint.

Apart from the theoretical and observed parameter correlations, we also encounter clear predictions regarding the observed parameters. The significance of Fig. 4 is apparent, as it underscores our model's claim and showcases that there is a wide spectrum of simultaneous values of θ_{23} for a single value of θ_{12}. Moving on, we further discuss the prediction of $\delta_{\rm CP}$ with mixing angles θ_{23} and θ_{12} as shown in Fig. 5. Here, we shown that $\delta_{\rm CP}$ is strongly correlated with θ_{23} and θ_{12}. Our model's
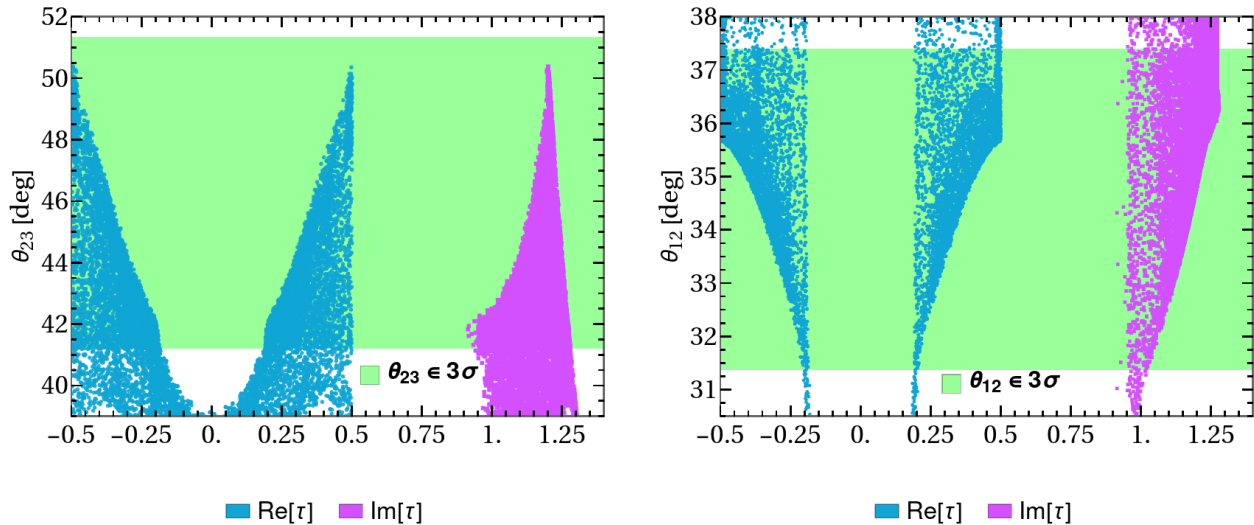
FIG. 3: Allowed values of $\mathrm{Re}[\tau]$ and $\mathrm{Im}[\tau]$ w.r.t. θ_{23} and θ_{12} when imposing other neutrino oscillation constraints in their 3σ region. The left panel corresponds to the correlation and limits on the $\mathrm{Re}[\tau]$ and $\mathrm{Im}[\tau]$ value with θ_{23} mixing angle. The right panel showcases the correlation of θ_{12} with $\mathrm{Re}[\tau]$ and $\mathrm{Im}[\tau]$.
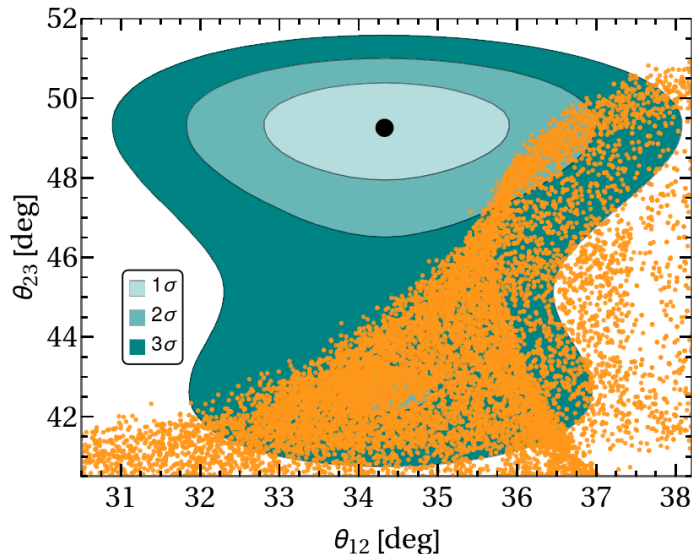

FIG. 4: In the above plot we discuss the correlation between θ_{23} and θ_{12} with their respective 3σ ranges.

predictions align closely with observations, remarkably near the 1σ region in the δ_{CP}-θ_{23} plane, and a margin of the 2σ region in the δ_{CP}-θ_{12} plane. Moreover, the correlation between δ_{CP} and θ_{23} can be tested in DUNE [112]. Significantly, our model's predictions manifest a distinctive feature: the inclination toward maximal CP violation. The striking insight from Fig. 5 is that the $\mathrm{Re}[\tau]$ values, whether negative or positive, yield two different solutions for δ_{CP}. Specifically, for $\mathrm{Re}[\tau] < 0$, δ_{CP} is predicted to be around $\frac{3\pi}{2}$, whereas $\mathrm{Re}[\tau] > 0$ leads to δ_{CP} to be around $\frac{\pi}{2}$. Consequently, the
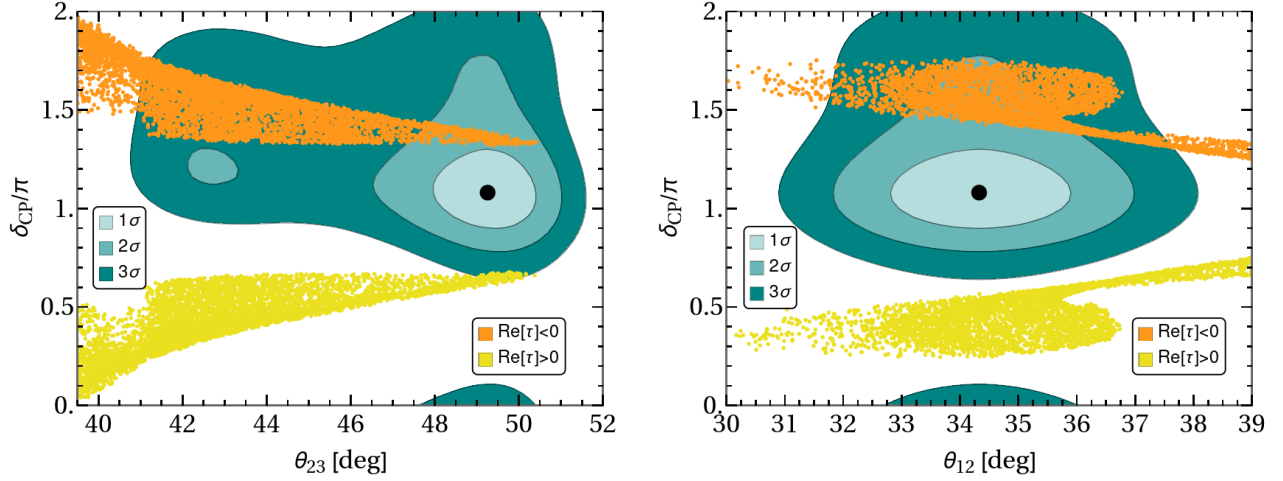
FIG. 5: Left panel corresponds to the correlation between $\delta_{\rm CP}$ and θ_{23} and right panel showcases the correlation between $\delta_{\rm CP}$ and θ_{12} with orange and yellow points valid for $-0.5 < {\rm Re}[\tau] < -0.2$ and $0.2 < {\rm Re}[\tau] < 0.5$, respectively.

preference for ${\rm Re}[\tau] < 0$ is evident when considering the implications of $\delta_{\rm CP}$ accordance with latest global-fit data [110, 111]. Note that the $\delta_{\rm CP}$ values in Fig. 5 show a reflection symmetry across $\delta_{\rm CP} = \pi$ value, which is a consequence of mirror symmetry exhibited by ${\rm Re}[\tau]$ across its value at zero as shown in Fig. 3.

3.2.   Prediction for Neutrinoless Double Beta ($0\nu\beta\beta$) Decay

In the context of the neutrinoless double beta decay process, the main contribution arising from the model to this process is due to the exchange of light neutrinos. The half life is proportional to the square of the effective mass $|m_{ee}|^2$, where $|m_{ee}|$ is given below in Eq. (17).

$$|m_{ee}| = |m_1 \cos^2 \theta_{12} \cos^2 \theta_{13} + m_2 \sin^2 \theta_{12} \cos^2 \theta_{13} e^{2i\phi_{12}} + m_3 \sin^2 \theta_{13} e^{2i\phi_{13}}| \, . \tag{17}$$

In our model, we have a very precise prediction for $0\nu\beta\beta$ as shown in the left panel of Fig. 6 in green color. The purple region represents the parameter space allowed by the latest global-fit data [110, 111] up to 3σ level, whereas constraint on the light neutrino mass arising from the *Planck* (TT, TE, EE + lowE + lensing + BAO) dataset, which has set an upper bound on the sum of neutrino masses $\sum m_i < 0.12$ eV [113] has been shown by the vertical gray band. Not only the neutrino masses are tightly constrained, but additionally, the Majorana phases are not free but highly correlated with each other, as shown in the right panel of Fig. 6. We also noted how Majorana phases correlation is related to ${\rm Re}[\tau]$ values. As a visual guide for the experimental searches of $0\nu\beta\beta$
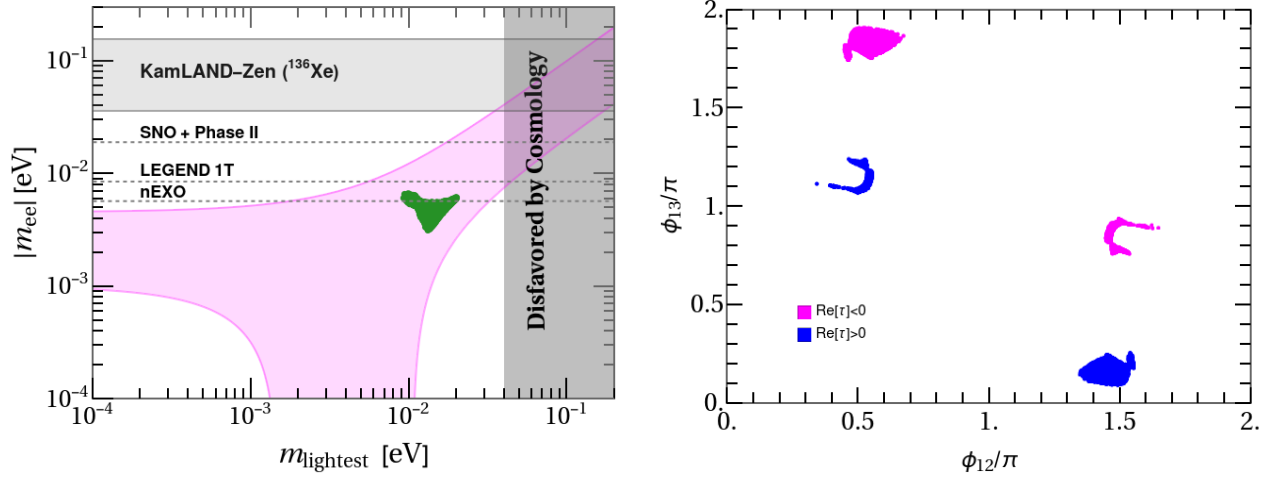
FIG. 6: The left panel corresponds to the effective neutrino mass $|m_{ee}|$ [eV] as a function of the lightest neutrino mass m_{lightest} [eV] predicting NO for neutrino mass while the right panel shows the correlation between Majorana phases.

decay, the horizontal gray band indicates the current experimental limits from KamLAND-Zen ($[36, 156]$ meV) [114], while the black-dashed lines correspond to the most optimistic sensitivities projected for SNO+ Phase II ($[19, 46]$ meV) [115], LEGEND 1000 ($[8.5, 19.4]$ meV) [116], nEXO ($[5.7, 17.7]$ meV) [117] at 90% C.L. Hence, our model can be tested in the upcoming years.
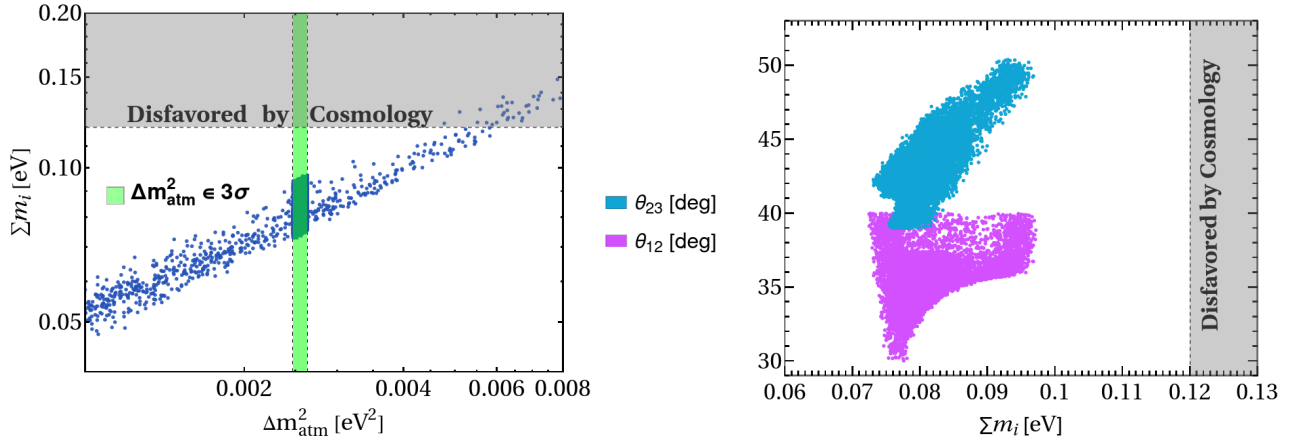
3.3. Cosmological Implications

FIG. 7: The left panel showcases the correlation between the sum of neutrino masses $\sum m_i$ with atmospheric mass square difference Δm_{atm}^2. While the right panel depicts the correlation of mixing angles θ_{23} and θ_{12} with $\sum m_i$.

Here, we delve into the cosmological implications arising from our model's predictions. The left panel of Fig. 7, serves to illustrate a robust correlation between the sum of neutrino masses ($\sum m_i$)
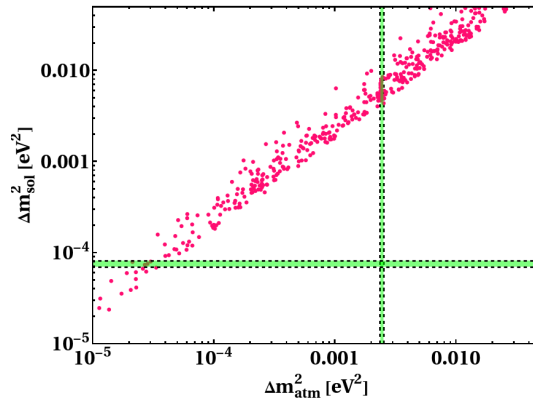
FIG. 8: Mass square differences (Δm^2_{sol} and Δm^2_{atm}) correlation in IO case.

and the atmospheric mass squared difference (Δm^2_{atm}). The green shaded region corresponds to the 3σ confidence level for Δm^2_{atm}, while the horizontal gray band denotes the upper limit on the sum of neutrino masses, $\sum m_i < 0.12$ eV [113]. It is worth noting that the constraint imposed by Δm^2_{atm} leads to a stringent bound on the sum of neutrino masses, confined within the range of $(0.073 - 0.097)$ eV, thus abiding by the established upper limit of 0.12 eV. However, it is imperative to emphasize that the Euclid mission, launched in July 2023, is expected to further constraint the sum of neutrino masses [118]. The right panel of Fig. 7 complements these revelations by suggesting a plausible correlation of the mixing angles θ_{23} and θ_{12} with the sum of neutrino masses $\sum m_i$.

3.4. Inverted Ordering (IO) Case

Following a modular setup in a scoto-seesaw scenario, it becomes evident that our framework encounters challenges in explaining the inverted ordering (IO) of neutrino mass. This limitation becomes apparent by looking at Fig. 8. We have shown a robust correlation between two mass square differences of neutrino oscillation, namely Δm^2_{sol} and Δm^2_{atm} in Fig. 8, while imposing 3σ constraint of all three mixing angles. The green shaded region represents the 3σ allowed values of Δm^2_{sol} and Δm^2_{atm}. Unfortunately, we can not satisfy both the mass square difference constraints simultaneously, as depicted in Fig. 8. Consequently, our model does not favor IO of neutrino mass.

4. LEPTON FLAVOR VIOLATIONS

In this section we explore our model's prediction for various lepton flavor violating processes.

4.1. Results for $\mu \to e\gamma$
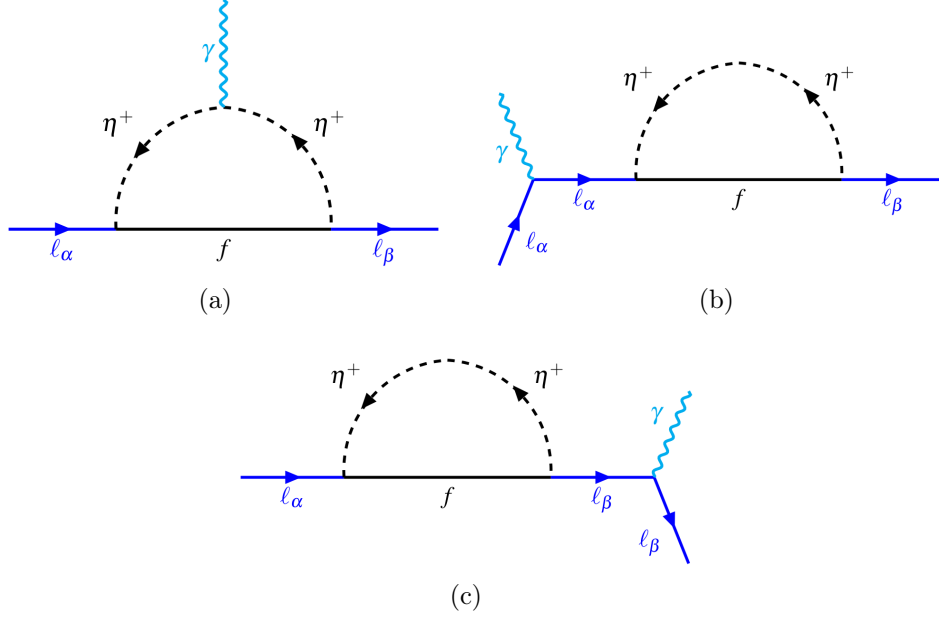

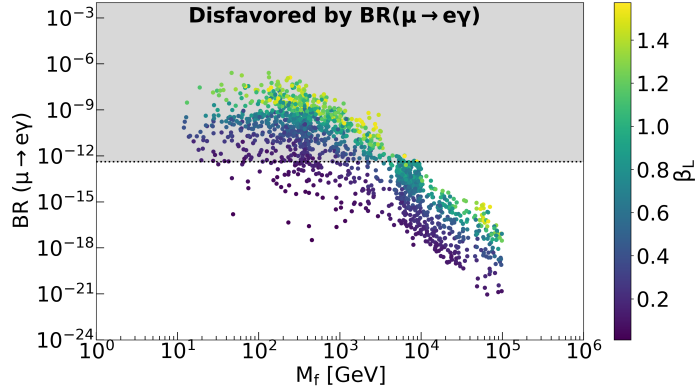FIG. 9: The panels 9(a), 9(b), 9(c) illustrates one loop Feynman diagrams for $l_\alpha \to l_\beta \gamma$.

FIG. 10: In this figure, we have condensed the expected values of the BR of $\mu \to e\gamma$ decay. These values are derived from the contributions detailed in Fig. 9. The colour bar located on the right side corresponds to the varying values of the free parameter β_L.

The quest for the lepton flavor-violating decay mode $\mu \to e\gamma$ holds significant importance in the exploration of new physics beyond the Standard Model. Numerous experiments are channeling substantial resources to enhance their sensitivity and improve the current limit on the branching ratio BR, denoted as BR($\mu \to e\gamma$). The present limit, established by the MEG collaboration [119] is less than 4.2×10^{-13}, which could reach to the sensitivity of 6×10^{-14} by the upgraded MEG i.e., MEG-II experiment [120]. In the existing theoretical framework, the process of lepton

flavor-violating decay $\mu \to e\gamma$ takes place at the one loop level through standard Yukawa interactions whose associated Feynman diagrams can be found in Fig. 9. The BR for the rare decay $\mu \to e\gamma$ is described in [121].

$$\mathrm{BR}(\mu \to e\gamma) = \frac{3(4\pi)^3\alpha}{4G_F^2}|\mathcal{A}_1|^2\mathrm{BR}(\mu \to e\overline{\nu}_e\nu_\mu), \tag{18}$$

where, $G_F \approx 10^{-5}~\mathrm{GeV}^{-2}$ is the Fermi constant, α being the electromagnetic fine structure constant and $\mathcal{A}_1$ is the dipole contribution, expressed as

$$\mathcal{A}_1 = \beta_L^2 \frac{Y_1^{(8)*}Y_{1''}^{(8)}}{32\pi^2}\frac{1}{m_{\eta^+}^2}\,\mathcal{G}_1\left(x\right). \tag{19}$$

Here, $Y_1^{(8)}$, $Y_{1''}^{(8)}$ being the modular Yukawa couplings, $x = \frac{M_f^2}{m_{\eta^+}^2}$ with m_η^+ being the mass of η^+ which we keep fixed at 400 GeV throughout our computation and $\mathcal{G}_1(x)$ is the loop function

$$\mathcal{G}_1(x) = \frac{1 - 6x + 3x^2 + 2x^3 - 6x^2\log x}{6(1-x)^4}\,. \tag{20}$$

In Fig. 10, we have depicted how the BR of $\mu \to e\gamma$ varies with respect to the mass of the fermion f. It is evident that as the value of β_L increases for a specific M_f value, the BR also exhibits an enhancement.

4.2. Results for $\mu \to 3e$

The three body LFV decay processes $\ell_\alpha \to \ell_\beta\overline{\ell_\beta}\ell_\beta$ can proceed through penguin and box diagrams, which are shown in Fig. 11. Our model supports the $\mu \to 3e$ decay and the corresponding branching ratio can be expressed as [121, 122],

$$\begin{aligned}\mathrm{BR}\left(\mu \to 3e\right) = \frac{2\pi^2\alpha^2}{G_F^2}&\left[3|\mathcal{A}_2|^2 + |\mathcal{A}_1|^2\left(16\log\left(r_{\mu e}\right) - 22\right) + \frac{1}{2}|\mathcal{B}_{box}|^2 + \left(2|F_{RR}|^2 + |F_{RL}|^2\right)\right.\\ &\left.+ \left(-6\mathcal{A}_2\mathcal{A}_1^* + \mathcal{A}_2\mathcal{B}_{box}^* - 2\mathcal{A}_1\mathcal{B}_{box}^* + h.c.\right)\right] \times \mathrm{BR}\left(\mu \to e\nu_\mu\overline{\nu}_e\right),\end{aligned} \tag{21}$$

where, $r_{\mu e} = \frac{m_\mu}{m_e}$ with F_{RR} and F_{RL} arising from the Z-boson contribution which are given as [122]

$$F_{RR} = \frac{\mathcal{F}_Z g_R^\ell}{g_2^2\sin^2\theta_W M_Z^2}, \quad F_{RL} = \frac{\mathcal{F}_Z g_L^\ell}{g_2^2\sin^2\theta_W M_Z^2}, \tag{22}$$
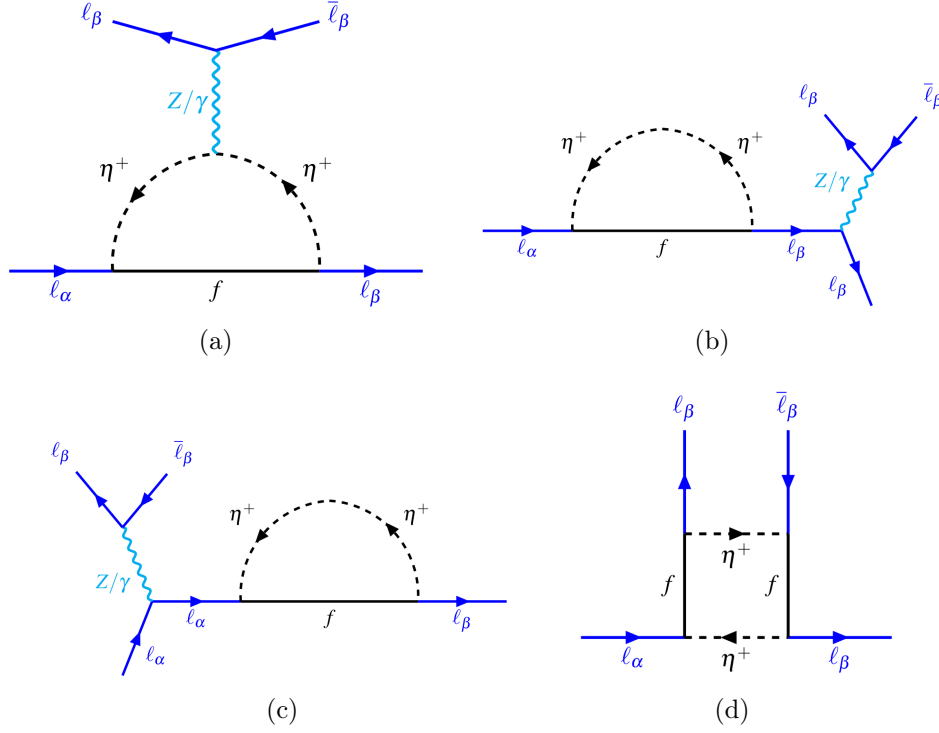
FIG. 11: The panels 11(a), 11(b), 11(c) and 11(d) represents the penguin diagrams and box diagram for $l_\alpha \to 3l_\beta$ respectively.

with

$$g_L^\ell = \frac{g_2}{\cos\theta_W}\left(\frac{1}{2} - \sin^2\theta_W\right), \quad g_R^\ell = -\frac{g_2}{\cos\theta_W}\sin^2\theta_W.$$ (23)

In this context, M_Z is the mass of the Z boson, g_2 represents the $SU(2)_L$ gauge coupling, and θ_W stands for the weak mixing angle. The coefficient $\mathcal{F}_Z$ is given below as

$$\mathcal{F}_Z = \beta_L^2 \frac{Y_1^{(8)*} Y_{1''}^{(8)}}{2(4\pi)^2} \frac{m_e m_\mu}{m_{\eta^+}^2} \frac{g_2}{\cos\theta_W} \mathcal{G}_2(x).$$ (24)

It is important to note that these terms are subjected to suppression by the masses of the charged leptons, m_e and m_μ. The form factor $\mathcal{A}_1$ is dipole contribution and is given in Eq. (19). The other form factor $\mathcal{A}_2$, given as

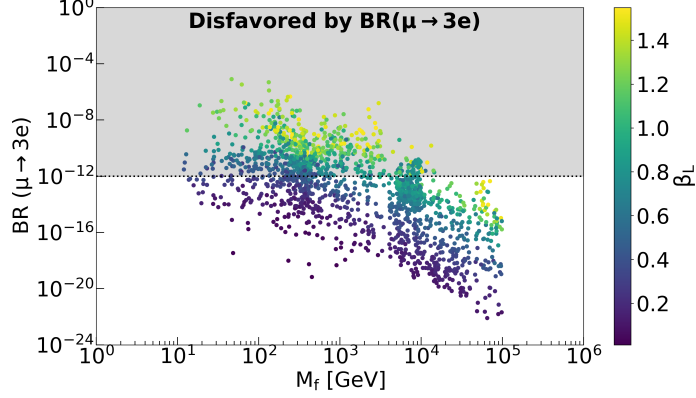$$\mathcal{A}_2 = \beta_L^2 \frac{Y_1^{(8)*} Y_{1''}^{(8)}}{6(4\pi)^2} \frac{1}{m_{\eta^+}^2} \mathcal{G}_2(x),$$ (25)

FIG. 12: Here, we have summarized the anticipated BR values for the $\mu \to 3e$ decay. These values are computed based on the contributions outlined in Fig. 11. The color bar positioned on the right side represents the changing values of the free parameter β_L.

can be generated by non-dipole contribution, whereas $\mathcal{B}_{\text{box}}$, induced by box diagrams, is given as

$$\mathcal{B}_{box} = \frac{\beta_L^2}{(4\pi e)^2 m_{\eta^+}^2} \left[\frac{1}{2} \mathcal{D}_1(x,x) + x\ \mathcal{D}_2(x,x) \right] Y_1^{(8)*} Y_1^{(8)*} Y_1^{(8)} Y_{1''}^{(8)} . \tag{26}$$

The loop functions $\mathcal{G}_2(x)$, $\mathcal{D}_1(x,x)$, and $\mathcal{D}_2(x,x)$ can be given as [121]

$$\mathcal{G}_2(x) = \frac{2 - 9x + 18x^2 - 11x^3 + 6x^3 \log x}{6(1-x)^4} , \tag{27}$$

$$\mathcal{D}_1(x,x) = \frac{-1 + x^2 - 2x \log x}{(1-x)^3} , \tag{28}$$

$$\mathcal{D}_2(x,x) = \frac{-2 + 2x - (1+x) \log x}{(1-x)^3} . \tag{29}$$

In the limit $x \to 1$, these loop functions have the values

$$\mathcal{G}_1(1) = \frac{1}{12}, \quad \mathcal{G}_2(1) = \frac{1}{4}, \quad \mathcal{D}_1(1,1) = -\frac{1}{3}, \quad \mathcal{D}_2(1,1) = \frac{1}{6} . \tag{30}$$

The current upper limit of BR($\mu \to 3e$) is 1×10^{-12}, while the upcoming Mu3e experiment [123] aims to achieve a remarkable sensitivity level of $\mathcal{O}(10^{-16})$, by adopting a phased strategy. Fig. 12 illustrates how the BR of $\mu \to 3e$ changes as a function of the fermion mass (M_f). Analogous to $\mu \to e\gamma$ process, the branching ratio increases with β_L for any specific value of M_f.
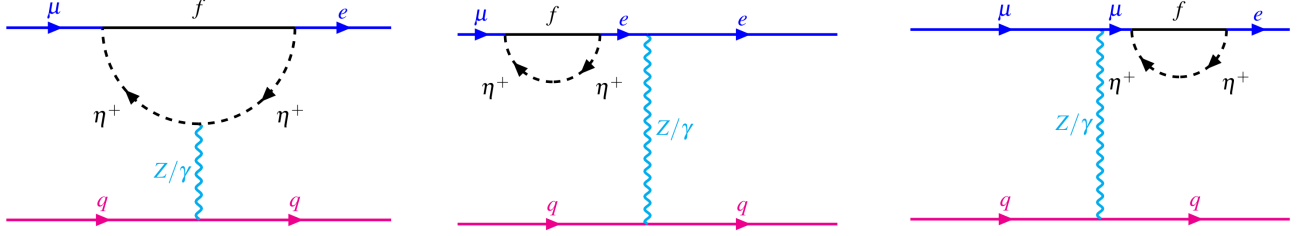
FIG. 13: Penguin contributions to $\mu - e$ conversion in nuclei.

4.3. $\mu - e$ conversion in Nuclei

The most stringent limitation on Lepton Flavor Violation (LFV) decays is currently represented by the $\mu \to e\gamma$ process. Nonetheless, we anticipate an enhanced level of sensitivity in the future, particularly from the $\mu - e$ conversion within the nucleus. Several experiments, such as Mu2e, DeeMe, COMET, and PRISM/PRIME [124–126], are currently at their peak aiming to establish an upper limit of 4.3×10^{-14} (for Titanium nucleus) and aspire to achieve future sensitivity as low as 10^{-18}. In the following, we provide a brief overview of the contribution arising from $\mu - e$ conversion in the nucleus, as depicted in Fig. 13. The conversion rate for $\mu - e$ within the nucleus is presented as follows:

$$
\begin{aligned}
\mathrm{CR}(\mu - e, \mathrm{Nucleus}) = {} & \frac{p_e \, E_e \, m_\mu^3 \, G_F^2 \, \alpha^3 \, Z_{\mathrm{eff}}^4 \, F_p^2}{8 \, \pi^2 \, Z \, \Gamma_{\mathrm{capt}}} \\
& \times \left\{ \left| (Z+N)\left(g_{LV}^{(0)} + g_{LS}^{(0)}\right) + (Z-N)\left(g_{LV}^{(1)} + g_{LS}^{(1)}\right) \right|^2 + \right. \\
& \left. \left| (Z+N)\left(g_{RV}^{(0)} + g_{RS}^{(0)}\right) + (Z-N)\left(g_{RV}^{(1)} + g_{RS}^{(1)}\right) \right|^2 \right\} .
\end{aligned}
\tag{31}
$$

Here, the proton and neutron numbers inside the nucleus are expressed by Z and N, Z_{eff} represents the effective atomic charge and can be found in [127] for different nuclei, F_p & Γ_{capt} denote the nuclear matrix element and the total muon capture rate respectively. These parameters can be determined based on the choice of the nucleus and can be found in Ref. [128, 129]. Other parameters used in the above equation are provided below, where $X = L, R$ and $K = V, S$:

$$
\begin{aligned}
g_{XK}^{(0)} &= \frac{1}{2} \sum_{q=u,d,s} \left(g_{XK(q)} G_K^{(q,p)} + g_{XK(q)} G_K^{(q,n)} \right) , \\
g_{XK}^{(1)} &= \frac{1}{2} \sum_{q=u,d,s} \left(g_{XK(q)} G_K^{(q,p)} - g_{XK(q)} G_K^{(q,n)} \right) .
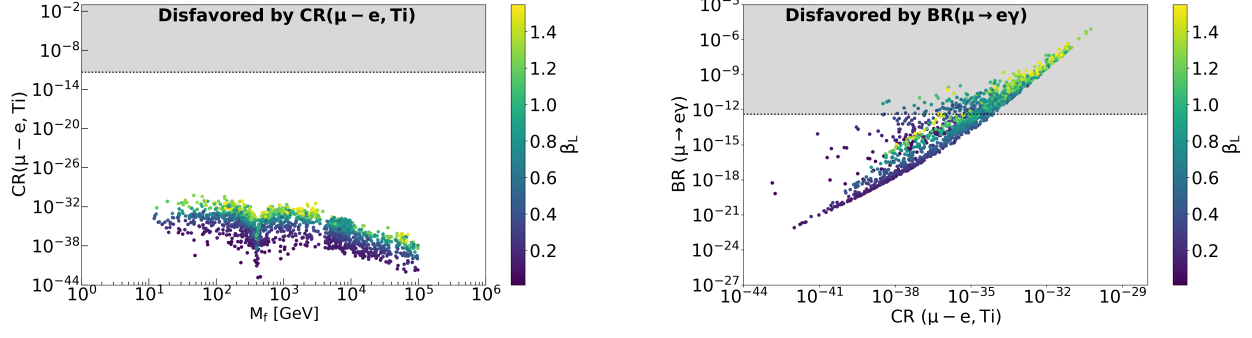\end{aligned}
\tag{32}
$$

FIG. 14: The left plot represents the variation of the conversion ratio of $\mu - e$ for Ti nucleus with the fermion mass M_f. However, the right plot elaborates the correlation between the conversion rate and BR for $\mu \to e\gamma$, with vertical and horizontal bands representing their respective upper bounds.

The numerical values of G_K coefficients are taken from [129–131]. Here, $g_{XK(q)}$ being the effective couplings, given as follows

$$
\begin{aligned}
g_{LS(q)} &\approx 0\,, \qquad g_{RS(q)} \approx 0\,, \\
g_{LV(q)} &\approx g^{\gamma}_{LV(q)} + g^{Z}_{LV(q)}\,, \\
g_{RV(q)} &= g_{LV(q)}\big|_{L \leftrightarrow R}\,,
\end{aligned}
\tag{33}
$$

where, $g^{\gamma}_{LV(q)} = \frac{\sqrt{2}}{G_F} e^2 \mathcal{Q}_q \left(\mathcal{A}_2 - \mathcal{A}_1 \right)$ is generated from photon penguins, $\mathcal{Q}_q$ represents electric charge of the corresponding quark, and

$$
g^{Z}_{LV(q)} = -\frac{\sqrt{2}}{G_F} \left(\frac{g^q_L + g^q_R}{2} \frac{\mathcal{F}_Z}{M^2_Z} \right)\,.
\tag{34}
$$

Further, g^q_L and g^q_R can be can be retrieved from Ref. [122]. We compute the conversion rate of $\mu - e$ in Titanium ($^{48}_{22}$Ti) nucleus (relevant details can be found in [129]). The left panel of Fig. 14 projects the conversion rate versus fermion mass M_f, and the right panel signifies its correlation with $\mathrm{BR}(\mu \to e\gamma)$. The horizontal dashed line corresponds to the upper bound [132].

Comments on Muon $g - 2$

In April 2021, Fermilab made a groundbreaking announcement with its inaugural measurement result [133] concerning the muon's anomalous magnetic dipole moment (referred to as $(g-2)_\mu$). When this result is combined with the findings from BNL [134], it reveals a substantial 4.2σ deviation from

the Standard Model prediction [135–137]. This remarkable deviation has significantly strengthened the confidence of particle physicists in their pursuit of uncovering new physics that extends beyond the Standard Model. In this context, we have identified three potential candidates, denoted as N_i, f, and η, in our model which could account for this anomaly. The individual contribution from N_i can be found in Ref. [138], revealing that due to the substantial mass of N_i, its contribution is exceedingly small. Furthermore, delving deeper into the analysis, the contributions of both f and η can be found from Ref. [139–142], demonstrating that they contribute negatively to the muon's anomalous magnetic moment. Moreover, our model is rooted in the Supersymmetric context and includes H_u and H_d, which can be viewed as a two-Higgs doublet model (2HDM) of type-II. However, it is worth noting that the contribution of this specific type of 2HDM does not align with experimental limitations [143–145].

Comments on Dark Matter

In our model, we have employed scoto-seesaw mechanism [59], wherein neutrino masses are generated through type-I seesaw at tree level and from scotogenic mechanism [109] at one loop level. The particles running inside the scoto-loop (η and f) can be potential DM candidate depending upon their masses. Here, the role of $\mathcal{Z}_2$ dark symmetry plays by the modular weight to stabilize the DM candidate. The dark sector particles, i.e., scalar η and fermion f, have odd modular weights while all other particles have even modular weights. Since Yukawa couplings can have only even weight [63], the dark sector particles do not mix with other particles. Therefore, the lightest of scalar η and fermion f will be a stable particle hence, a viable candidate for DM. The underlying dark matter phenomenology, in principle, aligns with the scoto-seesaw mechanism [59], where both the fermion and neutral scalar can be a DM candidate, hence, we do not discuss it in this paper.

5.   CONCLUSION

The primary objective of this paper is the introduction of A_4 modular symmetry in the context of neutrino phenomenology, employing the scoto-seesaw framework to explore its unique implications. We have achieved the generation of neutrino mass both at the tree level, utilizing right-handed neutrino superfields N_{R_i}, and at the one loop level, involving a fermion superfield f and an inert scalar doublet superfield η. Notably, the BSM fermions N_{R_i}, f and the inert scalar η are singlets under the A_4 symmetry, characterized by modular weights of 4, 5 and 3, respectively. To maintain

the invariance of the superpotential, we have harnessed higher-weight Yukawa couplings, which also are singlets under the A_4 symmetry, with modular weights of 4, 8, and 10, and are expressed in terms of lower-weight modular coupling, denoted as $Y_3^{(2)}$.

The utilization of modular symmetry offers several notable advantages, including eliminating the need for introducing additional flavon fields in the context of neutrino phenomenology, thereby enhancing the model's predictability. This approach enables attaining a distinct flavor structure within the neutrino mass matrix, encompassing neutrino mixing as well. As a result, our model is very predictive and has a robust correlation between the θ_{23} and θ_{12} mixing angles. Apart from this, we have strong correlation of $\delta_{\rm CP}$ with the mixing angles θ_{23} and θ_{12}. In addition, our model predicts normal ordering for neutrino masses, a narrow region for the lightest neutrino mass, $m_{\rm lightest} \in (9.2, 20.0) \times 10^{-3}$ eV and the sum of neutrino masses in the range of $\sum m_i \in (0.073, 0.097)$ eV. Similarly, for the neutrinoless double beta decay, we have very precise results predicting $|m_{ee}| \in (3.15, 6.66) \times 10^{-3}$ eV, which is within the potential reach of upcoming experiments. Furthermore, our investigation extends to evaluating the contributions of the present model to lepton flavor-violating decay, such as $\mu \to e\gamma$, ensuring compatibility with the stringent constraints set by the MEG collaboration. Additionally, we have explored processes like $\mu \to 3e$ and $\mu - e$ conversion for $\mathbf{Ti}$ nuclei within the framework of the current model. In conclusion, A_4 modular symmetry within the scoto-seesaw framework leads to a highly predictive model whose predictions can be tested in various experiments.

Appendix A: UV completion of SUSY scotogenic loop

To realize the scotogenic mechanism in our model we need the interaction of $(\eta^\dagger H_u)^2$ that provides mass splitting between real and imaginary components (η_R and η_I) of the scalar η. However, in the SUSY framework, such a term is not allowed. But, we can generate the mass splitting as an effective interaction. Here we discuss one possible way to generate this effective term in a UV complete model [146–148]. For the UV completion we have to add another superfield χ, which is a singlet under SM gauge symmetries. χ is also a singlet of A_4 with weight 5. The charge assignments and modular weight with additional superfield χ have been provided in Tab. III.

Fields	Fermions					Scalars			
	L_ℓ	ℓ^c_R	N_{R_1}	N_{R_2}	f	$H_{u,d}$	η	η'	χ
$SU(2)_L$	2	1	1	1	1	2	2	2	1
$U(1)_Y$	$-1/2$	1	0	0	0	$\pm 1/2$	$1/2$	$-1/2$	0
A_4	$1, 1', 1''$	$1, 1'', 1'$	1	$1'$	1	1	1	1	1
k_I	0	0	4	4	5	0	3	3	5

TABLE III: Particle content of the UV complete SUSY scotogenic loop.

The additional superpotential terms $\mathcal{W}_S$ are given as follows:

$$\mathcal{W}_S = \mu H_u H_d + \mu_\eta Y_1^{(6)} \eta \eta' + \frac{1}{2} \mu_\chi Y_1^{(10)} \chi \chi + \lambda_1 Y_1^{(8)} H_d \eta \chi + \lambda_2 Y_1^{(8)} H_u \eta' \chi.$$

The UV complete diagram has been shown in Fig. 15. These interactions will lead to a mass splitting between η_R and η_I. The diagrams shown in Fig. 15 generate neutrino masses at loop level through scotogenic mechanism in SUSY framework. The neutrino mass matrix at loop level can be expressed as:

$$\left(M_\nu^{ij} \right)_{\text{loop}} = \sum_{l=1}^{3} \mathcal{F}_{1l} M_f \mathbf{h^i h^j} + \sum_{l=1}^{3} \mathcal{F}_{2l} m_{\tilde{\eta}_l} \mathbf{h^i h^j} , \tag{A1}$$
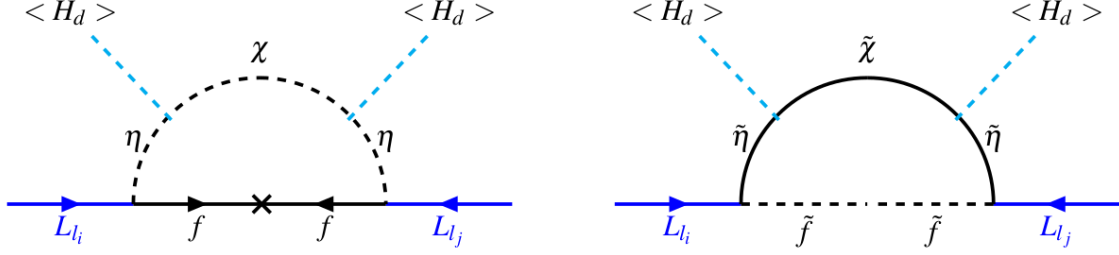
FIG. 15: Radiative neutrino mass generation in SUSY framework.

where $\mathcal{F}_{1l}$ and $\mathcal{F}_{2l}$ are the loop function given by:

$$\mathcal{F}_{1l} = \frac{1}{32\pi^2} \left[[U_R(2,l)]^2 \frac{m_{\eta Rl}^2}{M_f^2 - m_{\eta Rl}^2} \ln\left(\frac{M_f^2}{m_{\eta Rl}^2}\right) - [U_I(2,l)]^2 \frac{m_{\eta Il}^2}{M_f^2 - m_{\eta Il}^2} \ln\left(\frac{M_f^2}{m_{\eta Il}^2}\right) \right], \qquad (A2)$$

$$\mathcal{F}_{2l} = [U_\eta(2,l)]^2 \frac{1}{32\pi^2} \left[\frac{m_{fR}^2}{m_{\tilde{\eta}l}^2 - m_{fR}^2} \ln\left(\frac{m_{\tilde{\eta}l}^2}{m_{fR}^2}\right) - \frac{m_{fI}^2}{m_{\tilde{\eta}l}^2 - m_{fI}^2} \ln\left(\frac{m_{\tilde{\eta}l}^2}{m_{fI}^2}\right) \right]. \qquad (A3)$$

where, U_R and U_I are the orthogonal matrices that diagonalize the mass matrices constructed from real and imaginary components of (η, η', χ). Similarly, U_η diagonalizes the mass matrix of $(\tilde{\eta}, \tilde{\eta}',$ $\tilde{\chi})$. m_{fR} (m_{fI}) is the mass of the real (imaginary) component of $\tilde{f}$. The detailed discussion can be found in the Refs. [146–148].

In the limit $m_{\tilde{\eta}l} >> m_{fR,I}$, second term in Eq. (A1), $\mathcal{F}_{2l} m_{\tilde{\eta}l} \to 0$. Similarly, if masses of η' and χ are heavy, their contribution to neutrino mass is negligible. In this limit loop function $\mathcal{F}_{1l}$ can be expressed as follows:

$$\mathcal{F}_{1l} \to \mathcal{F} = \frac{1}{32\pi^2} \left[\frac{m_{\eta R}^2}{M_f^2 - m_{\eta R}^2} \ln\left(\frac{M_f^2}{m_{\eta R}^2}\right) - \frac{m_{\eta I}^2}{M_f^2 - m_{\eta I}^2} \ln\left(\frac{M_f^2}{m_{\eta I}^2}\right) \right]. \qquad (A4)$$

By considering $\tilde{f}$, η' and χ to be heavy, one can integrate them out. In the mass basis, the effective diagram of Fig. 15 will look like the right panel of Fig. 1. This effective interaction will induce mass splitting between η_R and η_I. From which neutrino masses will be generated effectively at loop level through scotogenic mechanism in SUSY framework.

Appendix B: A_4 Multiplication Rule

The symmetry group A_4 is an even permutation group of four objects. It has $4!/2=12$ elements and can be generated by two generators S and T obeying the relations:

$$S^2 = T^3 = (ST)^3 = \mathbb{I}.$$

The group has four irreducible representations: three singlets 1, 1', 1'', and a triplet 3. The product rules for the singlets and triplets are:

$$1 \otimes 1 = 1 = 1' \otimes 1'', \quad 1' \otimes 1' = 1'', \qquad 1'' \otimes 1'' = 1'.$$
$$3 \otimes 3 = 1 \oplus 1' \oplus 1'' \oplus 3_S \oplus 3_A. \tag{B1}$$

where, $3_{S(A)}$ denotes the symmetric (anti-symmetric) combination. In the complex basis where T is a diagonal matrix, we have following representation for S and T,

$$S = \frac{1}{3} \begin{pmatrix} -1 & 2 & 2 \\ 2 & -1 & 2 \\ 2 & 2 & -1 \end{pmatrix}, \qquad T = \begin{pmatrix} 1 & 0 & 0 \\ 0 & \omega & 0 \\ 0 & 0 & \omega^2 \end{pmatrix}, \tag{B2}$$

where, ω is the cubic root of unity. The product of two triplets $a = (a_1, a_2, a_3)$ and $b = (b_1, b_2, b_3)$ decomposes following Eq. (B1) and they are expressed as:

$$(ab)_1 = a_1 b_1 + a_2 b_3 + a_3 b_2,$$
$$(ab)_{1'} = a_3 b_3 + a_1 b_2 + a_2 b_1,$$
$$(ab)_{1''} = a_2 b_2 + a_3 b_1 + a_1 b_3,$$
$$(ab)_{3_S} = \frac{1}{\sqrt{3}} \begin{pmatrix} 2a_1 b_1 - a_2 b_3 - a_3 b_2 \\ 2a_3 b_3 - a_1 b_2 - a_2 b_1 \\ 2a_2 b_2 - a_3 b_1 - a_1 b_3 \end{pmatrix},$$
$$(ab)_{3_A} = \begin{pmatrix} a_2 b_3 - a_3 b_2 \\ a_1 b_2 - a_2 b_1 \\ a_3 b_1 - a_1 b_3 \end{pmatrix}. \tag{B3}$$

Appendix C: Modular forms of Yukawa Couplings

Here, we summarize our modular Yukawa construction in the context of A_4 symmetry. $\bar{\Gamma}$ is the modular group that attains a linear fractional transformation γ which acts on modulus τ linked to the upper-half complex plane whose transformation is given by

$$\tau \longrightarrow \gamma\tau = \frac{a\tau + b}{c\tau + d} , \quad \text{where} \;\; a, b, c, d \in \mathbb{Z} \;\; \text{and} \;\; ad - bc = 1, \;\; \text{Im}[\tau] > 0 , \tag{C1}$$

where it is isomorphic to the transformation $PSL(2, \mathbb{Z}) = SL(2, \mathbb{Z})/\{I, -I\}$. The S and T transformation helps in generating the modular transformation defined by

$$S : \tau \longrightarrow -\frac{1}{\tau} , \qquad T : \tau \longrightarrow \tau + 1 , \tag{C2}$$

and hence the algebraic relations so satisfied are as follows,

$$S^2 = \mathbb{I} , \qquad (ST)^3 = \mathbb{I} . \tag{C3}$$

Here, series of groups are introduced, $\Gamma(N)$ $(N = 1, 2, 3, \dots)$ and defined as

$$\Gamma(N) = \left\{ \begin{pmatrix} a & b \\ c & d \end{pmatrix} \in SL(2, \mathbb{Z}) , \quad \begin{pmatrix} a & b \\ c & d \end{pmatrix} = \begin{pmatrix} 1 & 0 \\ 0 & 1 \end{pmatrix} \;\; (\text{mod} N) \right\}. \tag{C4}$$

Definition of $\bar{\Gamma}(2) \equiv \Gamma(2)/\{I, -I\}$ for $N = 2$. Since $-I$ is not associated with $\Gamma(N)$ for $N > 2$ case, one can have $\bar{\Gamma}(N) = \Gamma(N)$, which are infinite normal subgroups of $\bar{\Gamma}$ known as principal congruence subgroups. Quotient groups come from the finite modular group, defined as $\Gamma_N \equiv \bar{\Gamma}/\bar{\Gamma}(N)$. The imposition of $T^N = \mathbb{I}$ is done for these finite groups Γ_N. Thus, the groups Γ_N $(N = 2, 3, 4, 5)$ are isomorphic to S_3, A_4, S_4 and A_5, respectively [61]. N level modular forms are holomorphic functions $f(\tau)$ which are transformed under the influence of $\Gamma(N)$ as follows:

$$f(\gamma\tau) = (c\tau + d)^k f(\tau) , \quad \gamma \in \Gamma(N) , \tag{C5}$$

where k is the modular weight.

Here, the discussion is all about the modular symmetric theory. This paper comprises of A_4 ($N = 3$) modular group. A field $\phi^{(I)}$ transforms under the modular transformation of Eq. (C1), as

$$\phi^{(I)} \rightarrow (c\tau + d)^{-k_I} \rho^{(I)}(\gamma) \phi^{(I)}, \tag{C6}$$

where $-k_I$ represents the modular weight and $\rho^{(I)}(\gamma)$ signifies an unitary representation matrix of $\gamma \in \Gamma(2)$.

The scalar fields' kinetic term is as follows

$$\sum_I \frac{|\partial_\mu \phi^{(I)}|^2}{(-i\tau + i\bar{\tau})^{k_I}}, \tag{C7}$$

which doesn't change under the modular transformation, and eventually, the overall factor is absorbed by the field redefinition. Thus, the Lagrangian should be invariant under the modular symmetry.

The modular forms of the Yukawa coupling $\mathbf{Y}_3^{(2)} = (y_1, y_2, y_3)$ with weight 2, which transforms as a triplet of A_4 can be expressed in terms of Dedekind eta-function $\eta(\tau)$ and its derivative [63]:

$$
\begin{aligned}
y_1(\tau) &= \frac{i}{2\pi} \left(\frac{\eta'(\tau/3)}{\eta(\tau/3)} + \frac{\eta'((\tau+1)/3)}{\eta((\tau+1)/3)} + \frac{\eta'((\tau+2)/3)}{\eta((\tau+2)/3)} - \frac{27\eta'(3\tau)}{\eta(3\tau)} \right), \\
y_2(\tau) &= \frac{-i}{\pi} \left(\frac{\eta'(\tau/3)}{\eta(\tau/3)} + \omega^2 \frac{\eta'((\tau+1)/3)}{\eta((\tau+1)/3)} + \omega \frac{\eta'((\tau+2)/3)}{\eta((\tau+2)/3)} \right), \\
y_3(\tau) &= \frac{-i}{\pi} \left(\frac{\eta'(\tau/3)}{\eta(\tau/3)} + \omega \frac{\eta'((\tau+1)/3)}{\eta((\tau+1)/3)} + \omega^2 \frac{\eta'((\tau+2)/3)}{\eta((\tau+2)/3)} \right).
\end{aligned}
\tag{C8}
$$

The Dedekind eta-function $\eta(\tau)$ is given by:

$$\eta(\tau) = q^{1/24} \prod_{n=1}^{\infty} (1 - q^n), \qquad q \equiv e^{i2\pi\tau}. \tag{C9}$$

In the form of q-expansion, the modular Yukawa of Eq. (C8) can be expressed as:

$$
\begin{aligned}
y_1(\tau) &= 1 + 12q + 36q^2 + 12q^3 + \cdots, \\
y_2(\tau) &= -6q^{1/3}(1 + 7q + 8q^2 + \cdots), \\
y_3(\tau) &= -18q^{2/3}(1 + 2q + 5q^2 + \cdots).
\end{aligned}
\tag{C10}
$$

From the q-expansion, we have the following constraint for modular Yukawa couplings:

$$y_2^2 + 2y_1 y_3 = 0. \tag{C11}$$

Higher modular weight Yukawa couplings can be constructed from weight 2 Yukawa $\mathbf{Y_3^{(2)}}$, using the A_4 multiplication rule. For modular weight $k = 4$, we have the following Yukawa couplings:

$$
\begin{aligned}
Y_3^{(4)} &= (y_1^2 - y_2 y_3,\, y_3^2 - y_1 y_2,\, y_2^2 - y_1 y_3), \\
Y_1^{(4)} &= y_1^2 + 2y_2 y_3, \\
Y_{1'}^{(4)} &= y_3^2 + 2y_1 y_2, \\
Y_{1''}^{(4)} &= y_2^2 + 2y_1 y_3.
\end{aligned} \tag{C12}
$$

At modular weight $k = 6$, the Yukawa couplings are:

$$
\begin{aligned}
Y_1^{(6)} &= y_1^3 + y_2^3 + y_3^3 - 3y_1 y_2 y_3, \\
Y_{3a}^{(6)} &= (y_1^3 + 2y_1 y_2 y_3,\, y_1^2 y_2 + 2y_2^2 y_3,\, y_1^2 y_3 + 2y_3^2 y_2), \\
Y_{3b}^{(6)} &= (y_3^3 + 2y_1 y_2 y_3,\, y_3^2 y_1 + 2y_1^2 y_2,\, y_3^2 y_2 + 2y_2^2 y_1), \\
Y_{3c}^{(6)} &= (y_2^3 + 2y_1 y_2 y_3,\, y_2^2 y_3 + 2y_3^2 y_1,\, y_2^2 y_1 + 2y_1^2 y_3).
\end{aligned} \tag{C13}
$$

Due to the constraint given in Eq. (C11), we see that $Y_{1''}^{(4)} = 0$ and $Y_{3c}^{(6)} = 0$. Similarly, we can construct other higher modular weight Yukawa. Here we are providing the relevant Yukawas of weights 8 and 10 given as follows:

$$
\begin{aligned}
Y_1^{(8)} &= \left(y_1^2 + 2y_2 y_3\right)^2, \\
Y_{1'}^{(8)} &= \left(y_1^2 + 2y_2 y_3\right)\left(y_3^2 + 2y_1 y_2\right), \\
Y_{1''}^{(8)} &= \left(y_3^2 + 2y_1 y_2\right)^2, \\
Y_1^{(10)} &= \left(y_1^2 + 2y_2 y_3\right)\left(y_1^3 + y_2^3 + y_3^3 - 3y_1 y_2 y_3\right).
\end{aligned} \tag{C14}
$$

In general, the dimension (d_k) of modular forms of the level 3 and weight k is $k + 1$ [63, 149]. The

Weight (k)	d_k	A_4 representations
2	3	**3**
4	5	**3**+**1**+**1′**
6	7	**3**+**3**+**1**
8	9	**3**+**3**+**1**+**1′**+**1″**
10	11	**3**+**3**+**3**+**1** +**1′**

TABLE IV: A_4 representations for different weight k.

representations for different weights are shown in Tab. IV.

---

[1] E. Ma, *Pathways to naturally small neutrino masses*, *Phys. Rev. Lett.* **81** (1998) 1171 [`hep-ph/9805219`].

[2] PARTICLE DATA GROUP collaboration, M. Tanabashi et al., *Review of Particle Physics*, *Phys. Rev. D* **98** (2018) 030001.

[3] R.N. Mohapatra and A.Y. Smirnov, *Neutrino Mass and New Physics*, *Ann. Rev. Nucl. Part. Sci.* **56** (2006) 569 [`hep-ph/0603118`].

[4] G. Altarelli and F. Feruglio, *Models of neutrino masses and mixings*, *New J. Phys.* **6** (2004) 106 [`hep-ph/0405048`].

[5] S.F. King, *Neutrino mass models*, *Rept. Prog. Phys.* **67** (2004) 107 [`hep-ph/0310204`].

[6] S. Weinberg, *Varieties of Baryon and Lepton Nonconservation*, *Phys. Rev. D* **22** (1980) 1694.

[7] S. Weinberg, *Baryon and Lepton Nonconserving Processes*, *Phys. Rev. Lett.* **43** (1979) 1566.

[8] F. Wilczek and A. Zee, *Operator Analysis of Nucleon Decay*, *Phys. Rev. Lett.* **43** (1979) 1571.

[9] P. Minkowski, $\mu \to e\gamma$ *at a Rate of One Out of* 10^9 *Muon Decays?*, *Phys. Lett.* **67B** (1977) 421.

[10] R.N. Mohapatra and G. Senjanovic, *Neutrino Mass and Spontaneous Parity Nonconservation*, *Phys. Rev. Lett.* **44** (1980) 912.

[11] M. Gell-Mann, P. Ramond and R. Slansky, *Complex Spinors and Unified Theories*, *Conf. Proc. C* **790927** (1979) 315 [`arXiv:1306.4669`].

[12] A. Zee, *A Theory of Lepton Number Violation, Neutrino Majorana Mass, and Oscillation*, *Phys. Lett.* **93B** (1980) 389.

[13] K.S. Babu, *Model of 'Calculable' Majorana Neutrino Masses*, *Phys. Lett. B* **203** (1988) 132.

[14] N. Arkani-Hamed, S. Dimopoulos, G.R. Dvali and J. March-Russell, *Neutrino masses from large*

extra dimensions, *Phys. Rev. D* **65** (2001) 024032 [`hep-ph/9811448`].

[15] D.V. Forero, C. Giunti, C.A. Ternes and O. Tyagi, *Large extra dimensions and neutrino experiments*, *Phys. Rev. D* **106** (2022) 035027 [`arXiv:2207.02790`].

[16] M. Carena, Y.Y. Li, C.S. Machado, P.A.N. Machado and C.E.M. Wagner, *Neutrinos in Large Extra Dimensions and Short-Baseline ν_e Appearance*, *Phys. Rev. D* **96** (2017) 095014 [`arXiv:1708.09548`].

[17] S. Roy, *Capability of the proposed long-baseline experiments to probe large extra dimension*, `arXiv:2305.16234`.

[18] L.A. Anchordoqui, I. Antoniadis and J. Cunat, *The Dark Dimension and the Standard Model Landscape*, `arXiv:2306.16491`.

[19] R.N. Mohapatra and J.W.F. Valle, *Neutrino Mass and Baryon Number Nonconservation in Superstring Models*, *Phys. Rev. D* **34** (1986) 1642.

[20] M.C. Gonzalez-Garcia and J.W.F. Valle, *Fast Decaying Neutrinos and Observable Flavor Violation in a New Class of Majoron Models*, *Phys. Lett. B* **216** (1989) 360.

[21] A.E. Cárcamo Hernández, J. Marchant González and U.J. Saldaña Salazar, *Viable low-scale model with universal and inverse seesaw mechanisms*, *Phys. Rev. D* **100** (2019) 035024 [`arXiv:1904.09993`].

[22] A. Abada, N. Bernal, A.E.C. Hernández, X. Marcano and G. Piazza, *Gauged inverse seesaw from dark matter*, *Eur. Phys. J. C* **81** (2021) 758 [`arXiv:2107.02803`].

[23] M.K. Behera and R. Mohanta, *Inverse seesaw in A_5' modular symmetry*, *J. Phys. G* **49** (2022) 045001 [`arXiv:2108.01059`].

[24] E. Ma and R. Srivastava, *Dirac or inverse seesaw neutrino masses from gauged $B\check{\,}L$ symmetry*, *Mod. Phys. Lett. A* **30** (2015) 1530020 [`arXiv:1504.00111`].

[25] M. Malinsky, J.C. Romao and J.W.F. Valle, *Novel supersymmetric SO(10) seesaw mechanism*, *Phys. Rev. Lett.* **95** (2005) 161801 [`hep-ph/0506296`].

[26] M.K. Behera and R. Mohanta, *Linear Seesaw in A5' Modular Symmetry With Leptogenesis*, *Front. in Phys.* **10** (2022) 854595 [`arXiv:2201.10429`].

[27] M. Sruthilaya, R. Mohanta and S. Patra, *A_4 realization of Linear Seesaw and Neutrino Phenomenology*, *Eur. Phys. J. C* **78** (2018) 719 [`arXiv:1709.01737`].

[28] M.K. Behera, S. Mishra, S. Singirala and R. Mohanta, *Implications of A4 modular symmetry on neutrino mass, mixing and leptogenesis with linear seesaw*, *Phys. Dark Univ.* **36** (2022) 101027 [`arXiv:2007.00545`].

[29] A. Batra, P. Bharadwaj, S. Mandal, R. Srivastava and J.W.F. Valle, *W-mass anomaly in the simplest linear seesaw mechanism*, *Phys. Lett. B* **834** (2022) 137408 [`arXiv:2208.04983`].

[30] A. Batra, P. Bharadwaj, S. Mandal, R. Srivastava and J.W.F. Valle, *Heavy neutrino signatures from leptophilic Higgs portal in the linear seesaw*, `arXiv:2304.06080`.

[31] A. Batra, P. Bharadwaj, S. Mandal, R. Srivastava and J.W.F. Valle, *Phenomenology of the simplest linear seesaw mechanism*, *JHEP* **07** (2023) 221 [`arXiv:2305.00994`].

[32] A.E. Cárcamo Hernández, V. K. N. and J.W.F. Valle, *Linear seesaw mechanism from dark sector*, *JHEP* **09** (2023) 046 [`arXiv:2305.02273`].

[33] A. Batra, H.B. Câmara and F.R. Joaquim, *Dark linear seesaw mechanism*, *Phys. Lett. B* **843** (2023) 138012 [`arXiv:2305.01687`].

[34] H. Zhang, *Light Sterile Neutrino in the Minimal Extended Seesaw*, *Phys. Lett. B* **714** (2012) 262 [`arXiv:1110.6838`].

[35] N. Nath, M. Ghosh, S. Goswami and S. Gupta, *Phenomenological study of extended seesaw model for light sterile neutrino*, *JHEP* **03** (2017) 075 [`arXiv:1610.09090`].

[36] S. Mishra, M.K. Behera, R. Mohanta, S. Patra and S. Singirala, *Neutrino phenomenology and dark matter in an A_4 flavour extended $B - L$ model*, *Eur. Phys. J. C* **80** (2020) 420 [`arXiv:1907.06429`].

[37] M. Kashav and S. Verma, *On minimal realization of topological Lorentz structures with one-loop seesaw extensions in A_4 modular symmetry*, *JCAP* **03** (2023) 010 [`arXiv:2205.06545`].

[38] S. Mishra, *Majorana dark matter and neutrino mass with S_3 symmetry*, *Eur. Phys. J. Plus* **135** (2020) 485 [`arXiv:1911.02255`].

[39] S. Verma, M. Kashav and S. Bhardwaj, *Highly predictive and testable A_4 flavor model within type-I and II seesaw framework and associated phenomenology*, *Nucl. Phys. B* **946** (2019) 114704 [`arXiv:1811.06249`].

[40] J. Ganguly, J. Gluza and B. Karmakar, *Common origin of θ_{13} and dark matter within the flavor symmetric scoto-seesaw framework*, *JHEP* **11** (2022) 074 [`arXiv:2209.08610`].

[41] A. Barman, N.K. Francis and H. Bora, *Neutrino Mixing Phenomenology: A_4 Discrete Flavor Symmetry with Type-I Seesaw Mechanism*, `arXiv:2306.11461`.

[42] D. Borah and B. Karmakar, *Linear seesaw for Dirac neutrinos with A_4 flavour symmetry*, *Phys. Lett. B* **789** (2019) 59 [`arXiv:1806.10685`].

[43] V.V. Vien and H.N. Long, *A_4-based model with linear seesaw scheme for lepton mass and mixing*, *Phys. Scripta* **98** (2023) 015301 [`arXiv:2302.03195`].

[44] V.V. Vien and N.V. Soi, *Fermion mass and mixing in an extension of the standard model with D_5 symmetry*, *Mod. Phys. Lett. A* **35** (2019) 2050003.

[45] V.V. Vien, *$3 + 1$ active–sterile neutrino mixing in $B - L$ model with $S_3 \times Z_4 \times Z_2$ symmetry for normal neutrino mass ordering*, *Eur. Phys. J. C* **81** (2021) 416.

[46] V.V. Vien, A.E.C. Hernández and H.N. Long, *Fermion masses and mixings in a U(1)X model based on the $\Sigma(18)$ discrete symmetry*, *PTEP* **2021** (2021) 083B02 [arXiv:2101.03506].

[47] P. Das, A. Mukherjee and M.K. Das, *Active and sterile neutrino phenomenology with A_4 based minimal extended seesaw*, *Nucl. Phys. B* **941** (2019) 755 [arXiv:1805.09231].

[48] S. Chuliá Centelles, R. Cepedello and O. Medina, *Absolute neutrino mass scale and dark matter stability from flavour symmetry*, *JHEP* **10** (2022) 080 [arXiv:2204.12517].

[49] C. Bonilla, J. Herms, O. Medina and E. Peinado, *Discrete dark matter mechanism as the source of neutrino mass scales*, *JHEP* **06** (2023) 078 [arXiv:2301.10811].

[50] M.K. Behera, P. Panda, P. Mishra, S. Singirala and R. Mohanta, *Exploring Neutrino Masses and Mixing in the Seesaw Model with $L_e - L_j$ Gauged Symmetry*, arXiv:2108.04066.

[51] P. Panda, M.K. Behera, P. Mishra and R. Mohanta, *Unveiling neutrino phenomenology, $(g - 2)_{e,\mu}$ and leptogenesis through U(1) gauge symmetries in an inverse seesaw model*, arXiv:2203.14536.

[52] A. Kamada, K. Kaneta, K. Yanagi and H.B. Yu, *Self-interacting dark matter and muon $g - 2$ in a gauged $U(1)_{L_\mu - L_\tau}$ model*, *JHEP* **06** (2018) 117 [arXiv:1805.00651].

[53] T. Araki, F. Kaneko, Y. Konishi, T. Ota, J. Sato and T. Shimomura, *Cosmic neutrino spectrum and the muon anomalous magnetic moment in the gauged $L_\mu - L_\tau$ model*, *Phys. Rev. D* **91** (2015) 037301 [arXiv:1409.4180].

[54] T. Nomura and T. Shimomura, *Search for Z' pair production from scalar boson decay in minimal $U(1)_{L_\mu - L_\tau}$ model at the LHC*, *Eur. Phys. J. C* **81** (2021) 297 [arXiv:2012.13049].

[55] S. Singirala, R. Mohanta and S. Patra, *Singlet scalar Dark matter in $U(1)_{B-L}$ models without right-handed neutrinos*, *Eur. Phys. J. Plus* **133** (2018) 477 [arXiv:1704.01107].

[56] A. Biswas, S. Choubey and S. Khan, *Inverse seesaw and dark matter in a gauged B-L extension with flavour symmetry*, *JHEP* **08** (2018) 062 [arXiv:1805.00568].

[57] A.B. McDonald, *Nobel lecture: The sudbury neutrino observatory: Observation of flavor change for solar neutrinos*, *Rev. Mod. Phys.* **88** (Jul, 2016) 030502, https://link.aps.org/doi/10.1103/RevModPhys.88.030502.

[58] T. Kajita, *Nobel lecture: Discovery of atmospheric neutrino oscillations*, *Rev. Mod. Phys.* **88** (Jul,

2016) 030501, https://link.aps.org/doi/10.1103/RevModPhys.88.030501.

[59] N. Rojas, R. Srivastava and J.W.F. Valle, *Simplest Scoto-Seesaw Mechanism*, *Phys. Lett. B* **789** (2019) 132 [arXiv:1807.11447].

[60] G.K. Leontaris and N.D. Tracas, *Modular weights, U(1)'s and mass matrices*, *Phys. Lett. B* **419** (1998) 206 [hep-ph/9709510].

[61] R. de Adelhart Toorop, F. Feruglio and C. Hagedorn, *Finite Modular Groups and Lepton Mixing*, *Nucl. Phys. B* **858** (2012) 437 [arXiv:1112.1340].

[62] T. Kobayashi, K. Tanaka and T.H. Tatsuishi, *Neutrino mixing from finite modular groups*, *Phys. Rev. D* **98** (2018) 016004 [arXiv:1803.10391].

[63] F. Feruglio, *Are neutrino masses modular forms?*, in *From My Vast Repertoire... Guido Altarelli's Legacy*, p. 227. World Scientific, 2019.

[64] G. Altarelli and F. Feruglio, *Discrete Flavor Symmetries and Models of Neutrino Mixing*, *Rev. Mod. Phys.* **82** (2010) 2701 [arXiv:1002.0211].

[65] T. Kobayashi and M. Tanimoto, *Modular flavor symmetric models*, 7, 2023, arXiv:2307.03384.

[66] H. Okada and Y. Orikasa, *Modular S_3 symmetric radiative seesaw model*, *Phys. Rev. D* **100** (2019) 115037 [arXiv:1907.04716].

[67] D. Meloni and M. Parriciatu, *A simplest modular S_3 model for leptons*, arXiv:2306.09028.

[68] S. Mishra, *Neutrino mixing and Leptogenesis with modular S_3 symmetry in the framework of type III seesaw*, arXiv:2008.02095.

[69] T. Nomura, H. Okada and H. Otsuka, *Texture zeros realization in a three-loop radiative neutrino mass model from modular A_4 symmetry*, arXiv:2309.13921.

[70] P. Mishra, M.K. Behera, P. Panda and R. Mohanta, *Type III seesaw under A_4 modular symmetry with leptogenesis*, *Eur. Phys. J. C* **82** (2022) 1115 [arXiv:2204.08338].

[71] X. Wang, *Lepton flavor mixing and CP violation in the minimal type-(I+II) seesaw model with a modular A_4 symmetry*, *Nucl. Phys. B* **957** (2020) 115105 [arXiv:1912.13284].

[72] M. Kashav and S. Verma, *Broken scaling neutrino mass matrix and leptogenesis based on A_4 modular invariance*, *JHEP* **09** (2021) 100 [arXiv:2103.07207].

[73] P. Mishra, M.K. Behera, P. Panda, M. Ghosh and R. Mohanta, *Exploring Models with Modular Symmetry in Neutrino Oscillation Experiments*, arXiv:2305.08576.

[74] J.N. Lu, X.G. Liu and G.J. Ding, *Modular symmetry origin of texture zeros and quark lepton unification*, *Phys. Rev. D* **101** (2020) 115020 [arXiv:1912.07573].

[75] T. Kobayashi, T. Nomura and T. Shimomura, *Type II seesaw models with modular A_4 symmetry*, *Phys. Rev. D* **102** (2020) 035019 [`arXiv:1912.00637`].

[76] T. Nomura, H. Okada and S. Patra, *An inverse seesaw model with A_4 -modular symmetry*, *Nucl. Phys. B* **967** (2021) 115395 [`arXiv:1912.00379`].

[77] M.K. Behera, S. Singirala, S. Mishra and R. Mohanta, *A modular A_4 symmetric scotogenic model for neutrino mass and dark matter*, *J. Phys. G* **49** (2022) 035002 [`arXiv:2009.01806`].

[78] B. Mitesh Kumar, *Phenomenological aspects of modular symmetry on neutrino mass models*, Ph.D. thesis, Hyderabad U., 2023.

[79] T. Nomura and H. Okada, *Quark and lepton model with flavor specific dark matter and muon $g-2$ in modular A_4 and hidden $U(1)$ symmetries*, `arXiv:2304.13361`.

[80] J. Kim and H. Okada, *Fermi-LAT GeV excess and muon $g-2$ in a modular A_4 symmetry*, `arXiv:2302.09747`.

[81] X.K. Du and F. Wang, *Flavor structures of quarks and leptons from flipped SU(5) GUT with A_4 modular flavor symmetry*, *JHEP* **01** (2023) 036 [`arXiv:2209.08796`].

[82] M.R. Devi, *Retrieving texture zeros in 3+1 active-sterile neutrino framework under the action of A_4 modular-invariants*, `arXiv:2303.04900`.

[83] A. Dasgupta, T. Nomura, H. Okada, O. Popov and M. Tanimoto, *Dirac Radiative Neutrino Mass with Modular Symmetry and Leptogenesis*, `arXiv:2111.06898`.

[84] T. Nomura, H. Okada and O. Popov, *A modular A_4 symmetric scotogenic model*, *Phys. Lett. B* **803** (2020) 135294 [`arXiv:1908.07457`].

[85] S. Centelles Chuliá, R. Kumar, O. Popov and R. Srivastava, *Neutrino Mass Sum Rules from Modular $\mathcal{A}_4$ Symmetry*, `arXiv:2308.08981`.

[86] J.T. Penedo and S.T. Petcov, *Lepton Masses and Mixing from Modular S_4 Symmetry*, *Nucl. Phys. B* **939** (2019) 292 [`arXiv:1806.11040`].

[87] P.P. Novichkov, J.T. Penedo, S.T. Petcov and A.V. Titov, *Modular S_4 models of lepton masses and mixing*, *JHEP* **04** (2019) 005 [`arXiv:1811.04933`].

[88] T. Kobayashi, Y. Shimizu, K. Takagi, M. Tanimoto and T.H. Tatsuishi, *A_4 lepton flavor model and modulus stabilization from S_4 modular symmetry*, *Phys. Rev. D* **100** (2019) 115045 [`arXiv:1909.05139`].

[89] X.G. Liu, C.Y. Yao and G.J. Ding, *Modular invariant quark and lepton models in double covering of S_4 modular group*, *Phys. Rev. D* **103** (2021) 056013 [`arXiv:2006.10722`].

[90] I. de Medeiros Varzielas, M. Levy, J.T. Penedo and S.T. Petcov, *Quarks at the modular S_4 cusp*, `arXiv:2307.14410`.

[91] G.J. Ding, S.F. King and C.Y. Yao, *Modular $S_4 \times SU(5)$ GUT*, *Phys. Rev. D* **104** (2021) 055034 [`arXiv:2103.16311`].

[92] S.F. King and Y.L. Zhou, *Trimaximal TM_1 mixing with two modular S_4 groups*, *Phys. Rev. D* **101** (2020) 015001 [`arXiv:1908.02770`].

[93] P.P. Novichkov, J.T. Penedo, S.T. Petcov and A.V. Titov, *Modular A_5 symmetry for flavour model building*, *JHEP* **04** (2019) 174 [`arXiv:1812.02158`].

[94] G.J. Ding, S.F. King and X.G. Liu, *Modular A_4 symmetry models of neutrinos and charged leptons*, *JHEP* **09** (2019) 074 [`arXiv:1907.11714`].

[95] T. Kobayashi, Y. Shimizu, K. Takagi, M. Tanimoto, T.H. Tatsuishi and H. Uchida, *Finite modular subgroups for fermion mass matrices and baryon/lepton number violation*, *Phys. Lett. B* **794** (2019) 114 [`arXiv:1812.11072`].

[96] X.G. Liu and G.J. Ding, *Neutrino Masses and Mixing from Double Covering of Finite Modular Groups*, *JHEP* **08** (2019) 134 [`arXiv:1907.01488`].

[97] P. Mishra, M.K. Behera and R. Mohanta, *Neutrino phenomenology, W-mass anomaly, and muon (g-2) in a minimal type-III seesaw model using a T' modular symmetry*, *Phys. Rev. D* **107** (2023) 115004 [`arXiv:2302.00494`].

[98] H. Okada and Y. Orikasa, *Lepton mass matrix from double covering of A_4 modular flavor symmetry**, *Chin. Phys. C* **46** (2022) 123108 [`arXiv:2206.12629`].

[99] X. Wang, B. Yu and S. Zhou, *Double covering of the modular A_5 group and lepton flavor mixing in the minimal seesaw model*, *Phys. Rev. D* **103** (2021) 076005 [`arXiv:2010.10159`].

[100] F. Feruglio, V. Gherardi, A. Romanino and A. Titov, *Modular invariant dynamics and fermion mass hierarchies around $\tau = i$*, *JHEP* **05** (2021) 242 [`arXiv:2101.08718`].

[101] P.P. Novichkov, J.T. Penedo, S.T. Petcov and A.V. Titov, *Generalised CP Symmetry in Modular-Invariant Models of Flavour*, *JHEP* **07** (2019) 165 [`arXiv:1905.11970`].

[102] C.Y. Yao, J.N. Lu and G.J. Ding, *Modular Invariant A_4 Models for Quarks and Leptons with Generalized CP Symmetry*, *JHEP* **05** (2021) 102 [`arXiv:2012.13390`].

[103] F. Feruglio, A. Strumia and A. Titov, *Modular invariance and the QCD angle*, *JHEP* **07** (2023) 027 [`arXiv:2305.08908`].

[104] D.M. Barreiros, F.R. Joaquim, R. Srivastava and J.W.F. Valle, *Minimal scoto-seesaw mechanism*

with spontaneous CP violation, JHEP **04** (2021) 249 [`arXiv:2012.05189`].

[105] D.M. Barreiros, F.R. Joaquim, R. Srivastava and J.W.F. Valle, *Neutrino Masses from Z8 Scoto-Seesaw Model with Spontaneous CP Violation*, in *Beyond Standard Model: From Theory to Experiment*, 2021, DOI.

[106] S. Mandal, R. Srivastava and J.W.F. Valle, *The simplest scoto-seesaw model: WIMP dark matter phenomenology and Higgs vacuum stability, Phys. Lett. B* **819** (2021) 136458 [`arXiv:2104.13401`].

[107] D.M. Barreiros, H.B. Camara and F.R. Joaquim, *Flavour and dark matter in a scoto/type-II seesaw model, JHEP* **08** (2022) 030 [`arXiv:2204.13605`].

[108] J. Leite, S. Sadhukhan and J.W.F. Valle, *Dynamical scoto-seesaw mechanism with gauged B − L*, `arXiv:2307.04840`.

[109] E. Ma, *Verifiable radiative seesaw mechanism of neutrino mass and dark matter, Phys. Rev.* **D73** (2006) 077301 [`hep-ph/0601225`].

[110] P.F. de Salas, D.V. Forero, S. Gariazzo, P. Martínez-Miravé, O. Mena, C.A. Ternes et al., *2020 global reassessment of the neutrino oscillation picture, JHEP* **02** (2021) 071 [`arXiv:2006.11237`].

[111] P. F. De Salas, D. V. Forero, S. Gariazzo, P. Martínez-Miravé, O. Mena, C. A. Ternes et al., *Chi2 profiles from Valencia neutrino global fit*, `http://globalfit.astroparticles.es/`, `https://doi.org/10.5281/zenodo.4726908`, 2021, 10.5281/zenodo.4726908.

[112] DUNE collaboration, B. Abi et al., *Deep Underground Neutrino Experiment (DUNE), Far Detector Technical Design Report, Volume II: DUNE Physics*, `arXiv:2002.03005`.

[113] PLANCK collaboration, N. Aghanim et al., *Planck 2018 results. VI. Cosmological parameters, Astron. Astrophys.* **641** (2020) A6 [`arXiv:1807.06209`].

[114] KAMLAND-ZEN collaboration, S. Abe et al., *First Search for the Majorana Nature of Neutrinos in the Inverted Mass Ordering Region with KamLAND-Zen*, `arXiv:2203.02139`.

[115] SNO+ collaboration, S. Andringa et al., *Current Status and Future Prospects of the SNO+ Experiment, Adv. High Energy Phys.* **2016** (2016) 6194250 [`arXiv:1508.05759`].

[116] LEGEND collaboration, N. Abgrall et al., *The Large Enriched Germanium Experiment for Neutrinoless ββ Decay: LEGEND-1000 Preconceptual Design Report*, `arXiv:2107.11462`.

[117] NEXO collaboration, J.B. Albert et al., *Sensitivity and Discovery Potential of nEXO to Neutrinoless Double Beta Decay, Phys. Rev. C* **97** (2018) 065503 [`arXiv:1710.05075`].

[118] L. Amendola et al., *Cosmology and fundamental physics with the Euclid satellite, Living Rev. Rel.* **21** (2018) 2 [`arXiv:1606.00180`].

[119] MEG collaboration, A.M. Baldini et al., *Search for the lepton flavour violating decay $\mu^+ \to e^+\gamma$ with the full dataset of the MEG experiment, Eur. Phys. J. C* **76** (2016) 434 [`arXiv:1605.05081`].

[120] MEG II collaboration, A.M. Baldini et al., *The Search for $\mu+ \to e+\gamma$ with 10–14 Sensitivity: The Upgrade of the MEG Experiment, Symmetry* **13** (2021) 1591 [`arXiv:2107.10767`].

[121] T. Toma and A. Vicente, *Lepton Flavor Violation in the Scotogenic Model, JHEP* **01** (2014) 160 [`arXiv:1312.2840`].

[122] A. Vicente and C.E. Yaguna, *Probing the scotogenic model with lepton flavor violating processes, JHEP* **02** (2015) 144 [`arXiv:1412.2545`].

[123] Mu3e collaboration, K. Arndt et al., *Technical design of the phase I Mu3e experiment, Nucl. Instrum. Meth. A* **1014** (2021) 165679 [`arXiv:2009.11690`].

[124] Mu2e collaboration, S. Miscetti, *Status of the Mu2e experiment at Fermilab, EPJ Web Conf.* **234** (2020) 01010.

[125] P. Dornan, *Mu to electron conversion with the COMET experiment, EPJ Web Conf.* **118** (2016) 01010.

[126] DeeMe collaboration, H. Natori, *An experiment to search for mu-e conversion at J-PARC MLF in Japan, DeeMe experiment, PoS* **ICHEP2018** (2019) 642.

[127] H.C. Chiang, E. Oset, T.S. Kosmas, A. Faessler and J.D. Vergados, *Coherent and incoherent (mu-, e-) conversion in nuclei, Nucl. Phys. A* **559** (1993) 526.

[128] R. Kitano, M. Koike and Y. Okada, *Detailed calculation of lepton flavor violating muon electron conversion rate for various nuclei, Phys. Rev. D* **66** (2002) 096002 [`hep-ph/0203110`].

[129] E. Arganda, M.J. Herrero and A.M. Teixeira, *mu-e conversion in nuclei within the CMSSM seesaw: Universality versus non-universality, JHEP* **10** (2007) 104 [`arXiv:0707.2955`].

[130] Y. Kuno and Y. Okada, *Muon decay and physics beyond the standard model, Rev. Mod. Phys.* **73** (2001) 151 [`hep-ph/9909265`].

[131] T.S. Kosmas, S. Kovalenko and I. Schmidt, *Nuclear muon- e- conversion in strange quark sea, Phys. Lett. B* **511** (2001) 203 [`hep-ph/0102101`].

[132] SINDRUM II collaboration, C. Dohmen et al., *Test of lepton flavor conservation in mu —> e conversion on titanium, Phys. Lett. B* **317** (1993) 631.

[133] Muon g-2 collaboration, B. Abi et al., *Measurement of the Positive Muon Anomalous Magnetic Moment to 0.46 ppm, Phys. Rev. Lett.* **126** (2021) 141801 [`arXiv:2104.03281`].

[134] Muon g-2 collaboration, G.W. Bennett et al., *Final Report of the Muon E821 Anomalous Magnetic*

Moment Measurement at BNL, *Phys. Rev. D* **73** (2006) 072003 [`hep-ex/0602035`].

[135] M. Davier, A. Hoecker, B. Malaescu and Z. Zhang, *Reevaluation of the Hadronic Contributions to the Muon g-2 and to alpha(MZ)*, *Eur. Phys. J. C* **71** (2011) 1515 [`arXiv:1010.4180`].

[136] M. Davier, A. Hoecker, B. Malaescu and Z. Zhang, *Reevaluation of the hadronic vacuum polarisation contributions to the Standard Model predictions of the muon $g-2$ and $\alpha(m_Z^2)$ using newest hadronic cross-section data*, *Eur. Phys. J. C* **77** (2017) 827 [`arXiv:1706.09436`].

[137] T. Aoyama et al., *The anomalous magnetic moment of the muon in the Standard Model*, *Phys. Rept.* **887** (2020) 1 [`arXiv:2006.04822`].

[138] J.P. Leveille, *The Second Order Weak Correction to (G-2) of the Muon in Arbitrary Gauge Models*, *Nucl. Phys. B* **137** (1978) 63.

[139] F.S. Queiroz and W. Shepherd, *New Physics Contributions to the Muon Anomalous Magnetic Moment: A Numerical Code*, *Phys. Rev. D* **89** (2014) 095024 [`arXiv:1403.2309`].

[140] L. Calibbi, R. Ziegler and J. Zupan, *Minimal models for dark matter and the muon $g-2$ anomaly*, *JHEP* **07** (2018) 046 [`arXiv:1804.00009`].

[141] S. Jana, P.K. Vishnu, W. Rodejohann and S. Saad, *Dark matter assisted lepton anomalous magnetic moments and neutrino masses*, *Phys. Rev. D* **102** (2020) 075003 [`arXiv:2008.02377`].

[142] D. Borah, M. Dutta, S. Mahapatra and N. Sahu, *Lepton anomalous magnetic moment with singlet-doublet fermion dark matter in a scotogenic U(1)Lµ-Lτ model*, *Phys. Rev. D* **105** (2022) 015029 [`arXiv:2109.02699`].

[143] A. Broggio, E.J. Chun, M. Passera, K.M. Patel and S.K. Vempati, *Limiting two-Higgs-doublet models*, *JHEP* **11** (2014) 058 [`arXiv:1409.3199`].

[144] L. Wang and X.F. Han, *A light pseudoscalar of 2HDM confronted with muon g-2 and experimental constraints*, *JHEP* **05** (2015) 039 [`arXiv:1412.4874`].

[145] S. Iguro, T. Kitahara, M.S. Lang and M. Takeuchi, *Current Status of the Muon g-2 Interpretations within Two-Higgs-Doublet Models*, `arXiv:2304.09887`.

[146] E. Ma, *Supersymmetric Model of Radiative Seesaw Majorana Neutrino Masses*, *Annales Fond. Broglie* **31** (2006) 285 [`hep-ph/0607142`].

[147] E. Ma, *SU(5) completion of the dark scalar doublet model of radiative neutrino mass*, *Phys. Lett. B* **659** (2008) 885 [`arXiv:0710.2325`].

[148] R.S. Hundi, *$\mu \to e\gamma$ in a supersymmetric radiative neutrino mass model*, *Phys. Rev. D* **93** (2016) 015008 [`arXiv:1510.02253`].

[149] S. Kikuchi, T. Kobayashi, H. Otsuka, M. Tanimoto, H. Uchida and K. Yamamoto, *4D modular flavor symmetric models inspired by a higher-dimensional theory*, *Phys. Rev. D* **106** (2022) 035001 [`arXiv:2201.04505`].